AD-A157 078 NUMERICAL AND EXPERIMENTAL STUDIES OF 3-D AND UNSTEADY TURBULENT BODY/APP..(U) VIRGINIA POLYTECHNIC INST AND STATE UNIV BLACKSBURG DEPT OF A.. J A SCHETZ ET AL. 1/1

UNCLASSIFIED 15 JUN 85 N00014-83-K-0372 F/G 20/4 NL

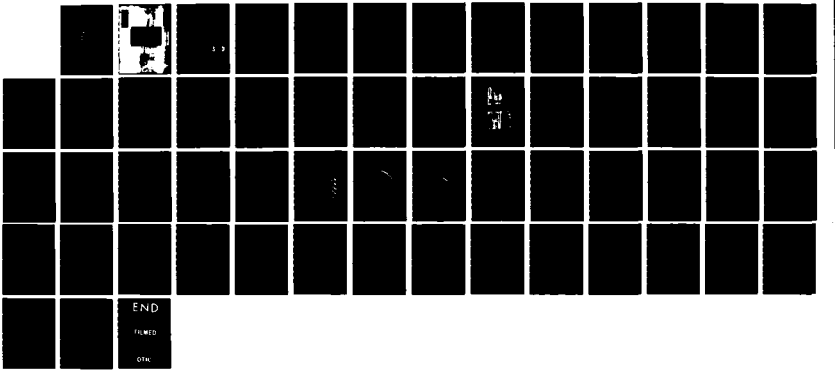

Annual Report No. 2 15 June 1985

Contract N00014-83-K-0372; NR 657-738/3-4-83 (4929)

NUMERICAL AND EXPERIMENTAL STUDIES OF 3-D AND UNSTEADY TURBULENT BODY/APPENDAGE/PROPELLER FLOWS

J.A. Schetz and R.L. Simpson
Aerospace and Ocean Engineering Department

Annual Report for Period 15 May 1984 - 14 May 1985

Prepared for

Annual Report No. 2 15 June 1985

Contract N00014-83-K-0372; NR 657-732/3-4-83 (432F)

NUMERICAL AND EXPERIMENTAL STUDIES OF 3-D AND UNSTEADY TURBULENT BODY/APPENDAGE/PROPELLER FLOWS

J.A. Schetz and R.L. Simpson
Aerospace and Ocean Engineering Department

Annual Report for Period 15 May 1984 - 14 May 1985

Prepared for
Office of NAVAL RESEARCH
800 N. Quincy St.
Arlington, VA 22217

UNCLASSIFIED
SECURITY CLASSIFICATION OF THIS PAGE (When Data Entered)

REPORT DOCUMENTATION PAGE		READ INSTRUCTIONS BEFORE COMPLETING FORM
1. REPORT NUMBER	2. GOVT ACCESSION NO. AD-A157 078	3. RECIPIENT'S CATALOG NUMBER
4. TITLE (and Subtitle) NUMERICAL AND EXPERIMENTAL STUDIES OF 3-D AND UNSTEADY TURBULENT BODY/APPENDAGE/PROPELLER FLOWS		5. TYPE OF REPORT & PERIOD COVERED Annual Report 15 May 1984 - 14 May 1985
		6. PERFORMING ORG. REPORT NUMBER Annual Report No. 2
7. AUTHOR(s) J. A. Schetz and R. L. Simpson		8. CONTRACT OR GRANT NUMBER(s) N00014-83-K-0372
9. PERFORMING ORGANIZATION NAME AND ADDRESS Aerospace and Ocean Engineering Department Virginia Polytechnic Institute and State Univ. Blacksburg, VA 24061		10. PROGRAM ELEMENT, PROJECT, TASK AREA & WORK UNIT NUMBERS
11. CONTROLLING OFFICE NAME AND ADDRESS Office of Naval Research 800 No. Quincy St. Arlington, VA 22217		12. REPORT DATE 15 June 1985
		13. NUMBER OF PAGES
14. MONITORING AGENCY NAME & ADDRESS(if different from Controlling Office)		15. SECURITY CLASS. (of this report) Unclassified
		15a. DECLASSIFICATION/DOWNGRADING SCHEDULE

16. DISTRIBUTION STATEMENT (of this Report)
Approved for public release; distribution unlimited. Reproduction in whole or in part is permitted for any purpose of the United States Government.

17. DISTRIBUTION STATEMENT (of the abstract entered in Block 20, if different from Report)

18. SUPPLEMENTARY NOTES

19. KEY WORDS (Continue on reverse side if necessary and identify by block number)
Propeller Flowfields ;
Appendage Flows ;
Numerical Solutions of Turbulent Flows .

20. ABSTRACT (Continue on reverse side if necessary and identify by block number)
The 3-D, turbulent flowfield produced by a propeller operating in the wake of a variable mesh disk has been studied with numerical solutions of the Reynolds-averaged, Navier-Stokes equations and by detailed experiments in a wind tunnel. The mesh variations of the upstream disk were chosen to produce a simulation of the wake of a streamlined, axisymmetric body with a single, streamlined appendage. Comparisons of measurements and preliminary numerical predictions show good agreement for the velocity profiles behind the propeller.

DD FORM 1 JAN 73 1473 EDITION OF 1 NOV 65 IS OBSOLETE

UNCLASSIFIED
SECURITY CLASSIFICATION OF THIS PAGE (When Data Entered)

Abstract continued Block 20

The 3-D flow in the junction between a cylindrical appendage and a hull can produce separation on the trailing portion of the appendage and produces a momentum deficient 3-D boundary layer that is more prone to detachment than the 2-D regions away from the appendage. Detailed measurements of the zero-pressure-gradient boundary layer upstream of an appendage of interest have been made. A procedure has been developed for reducing blockage effects in the test wind tunnel. Keywords: → (to A)

Table of Contents

INTRODUCTION

Analysis and detailed understanding of the flowfield produced by a propeller/body/appendage combination is of interest in a number of practical applications. Examples include the influence of the propeller on the body pressure distribution to estimate the thrust deduction, the effects of non-uniform inflow on propeller performance, the prediction of the near-wake profiles, cyclic loading to produce vibrations and unsteady bearing forces and the influence of a rudder or other appendages on the propeller and vice versa. We have been conducting a research plan that addresses two important parts of the general problem: 1) numerical analysis of the 3-D, turbulent flow produced by propeller/body/appendage combinations and 2) studies of the large-scale and unsteady structure of 3-D, turbulent boundary layer flows produced by hull/appendage junctions. This section contains some background material on these research areas.

Numerical Solution of 3-D, Turbulent Propeller Flows

We consider first the current state of knowledge for analysis of 3-D, turbulent flows near and through propellers. Until quite recently, only approximate treatments, e.g., Refs. (1) - (5) were available. These analyses involved one or more of the following restrictive assumptions: the flow was assumed inviscid; the propeller was represented as an actuator disk with constant thrust over the disk; the flow was taken as laminar and/or the effects of the propeller on the flowfield were assumed small enough to permit a linearization of the equations of motion.

The numerical solution procedure reported in Refs. (6) and (7) had as its goal the development of a realistic treatment, holding simplifying assumptions and approximations to a minimum. The work was based on the

full, axisymmetric, mean (in the turbulence sense), unsteady Navier-Stokes equations. In order to place some bounds on the scope of the effort, however, some simplifications were necessary. The first was the assumption of an actuator disk model for the propeller, although arbitrary radial variations of thrust were allowed. Second, the flow was taken as axisymmetric. Third, turbulent transport processes were described by an integrated, turbulence-kinetic-energy (TKE) equation, which was used to predict an eddy viscosity distribution. The eddy viscosity was allowed to vary only in the streamwise direction. The simulation of a given propeller for the purposes of a viscous numerical calculation was considered in detail for the first time in this work. The unsteady equations of motion were cast in terms of a stream function, one vorticity component, and the peripheral velocity. The vorticity equation and the peripheral momentum equation were solved by an Alternating Difference Implicit technique, and the Poisson equation for the stream function was solved by Direct Matrix Reduction.

Comparison of the predictions of that procedure with laboratory data for an axisymmetric, slender, upstream body with no appendages showed good agreement for the axial velocity profile at X/D = 2. The swirl velocity component was underpredicted.

From the point of view of direct applications to problems of practical interest, the biggest limitation to the analysis described above is that it was restricted to two-dimensional, axisymmetric flows. Actual propeller-driven vessels have either a three-dimensional body ahead of the propeller and/or appendages such as rudders or control planes near the propeller that render the flow basically three-dimensional, even if the propeller is still taken as an actuator disk, neglecting the explicit influence of individual blades. For many cases, the assumption of an actuator disk representation

of the propeller remains appropriate while the restriction to axisymmetric flows does not.

The research program undertaken in 1983 under ONR support is a step-by-step approach to the development of a method for handling propeller flowfields with three-dimensional inflows and the effects of appendages in situations of increasing complexity and practical realism, while retaining a general actuator disk model of the propeller. The problem treated in the first year was an isolated propeller operating in an approach flow with a linear velocity gradient. The numerical solution procedure was based on the Finite Element Method (FEM) for the steady Navier-Stokes equations written in primitive variables following the suggestions of Engelman (Refs. (8), (9) and (10)). Turbulence modeling was through an integrated form of the Turbulent Kinetic Energy (TKE) equation. In order to have flowfield measurements against which the adequacy of the numerical predictions could be tested, a series of wind tunnel experiments was run.

Calculations have been run for two cases where experimental data are available - one with a uniform approach velocity as a baseline case and one with the linear velocity gradient approach velocity profile. Comparisons of predictions and measurements are given in Ref. (11) (see the report in the Appendix) for streamwise velocity profiles just behind the propeller disk (X/D = .025). The numerical (FEM) predictions give a good description of the flow.

3-D Turbulent Flows from Hull Appendage Junctions

When a laminar or turbulent boundary layer on a surface encounters a protuberance of strut projecting from that surface, a "horseshoe" vortex is formed at the junction of the two surfaces. Upstream of the protuberance

the time-averaged vorticity direction in the boundary layer is spanwise across the surface. In order to satisfy the vortex theorems of fluid dynamics, streamwise legs of this upstream vorticity stretch around the protuberance in a horseshoe shape with each leg having vorticity of opposite rotational sense. This type of three-dimensional turbulent boundary layer occurs in a number of practical cases, such as in turbomachinery blade and end wall flows, aircraft wing and body junction flows, and ship appendage and hull junction flow.

Dean (Ref. 12) and Humphreys and vandenBerg (Ref. 13) reviewed available data for this type of flow in order to select the best test cases for evaluating computational methods (Ref. 14). Dean pointed out that little turbulence data had been obtained during 50 years of measurements. Consequently, only the Shabaka (Ref. 15) flow around a flat plate with a semi-elliptical nose was recommended as a computational test case for the secondary flow produced by the streamwise vortex legs well downstream of the nose. Humphreys and vandenBerg recommended the Dechow (Ref. 16) flow as a test case, in which turbulence measurements were made in front of and beside the protuberance or obstruction, but not in the presence of adverse pressure gradients. In this case the protuberance was a 320 mm diameter semi-circular cylinder with a streamlined afterbody that prevented premature separation upstream of the trailing edge. Pierce's group (Ref. 17) have made some time-averaged measurements around the nose of a circular-nosed strut.

From a computational viewpoint, the nose region is the easiest to calculate since the incident boundary layer mean vorticity distribution and an inviscid rotational solution technique largely determine the rapidly distorted flowfield around the nose. Computational methods for the mean

flow in the corners around a protuberance are not in a satisfactory state, even for the zero pressure gradient case (Ref. 14). Dean pointed out the need for measurements of the streamwise vortex corner flow in the presence of adverse pressure gradients for increased understanding and for improvement and verification of computational methods. In most practical applications these adverse pressure gradients cause the vortex strength to be attenuated and the vortex to wander away from the corner (Ref. 19).

In other work on streamlined struts, Barber (Ref. 20) showed that the size of the separated flow zone was inversely related to the incident boundary layer thickness. Mehta (unpublished, but referenced in Ref. 19) showed that the streamwise corner vortex diameter and distance from the body were dependent on the leading-edge shape. Recently, Oguz (Ref. 21) made measurements on the flow around a body of constant thickness, a case similar to Shabaka's.

In all of these studies only time-averaged measurements were made. No quantitative measurements were made of flow regions that contain adverse pressure gradients and/or separation. No spectra of the turbulence energy containing frequencies were obtained. No examination has been made of the organized time-varying coherent structure of this type of turbulent boundary layer, such as has been done for mean two-dimensional turbulent boundary layers.

Recently, Rood at DWTNSRDC reported relatively narrow frequency bandwidth turbulent fluctuations in the three-dimensional boundary layer downstream of a streamlined protuberance. In some cases this downstream boundary layer passes over other protuberances and structural elements and interacts with them in an undesirable and as yet unpredictable way. Noise is generated when large-scale turbulent structures in this boundary layer

interact with these structural elements. When a rotor blade encounters the wake of a strut, tonal noise is generated. It is thought that the organized time-varying coherent structure of these flows may be able to explain such undesirable behavior and to aid in future optimal designs of these structural elements.

A time-averaged description of the three-dimensional flow downstream of a protuberance, whether from experiments or a calculation method, provides no information on the large-scale time-dependent motions. Since these large-scale time-dependent motions would interact with downstream moving rotor blades differently than for the mean flow, information is needed on the nature of these large-scale structures of a three-dimensional flow downstream of a protuberance.

Thus, although there have been previous time-averaged measurements of this type of flow in flow regions without pressure gradients or separation, there has been no investigation of the role of the time-dependent organized turbulent flow structure, and no quantitative measurements of flow regions that contain adverse pressure gradients and/or separation.

At this time we can only conjecture about how a protuberance affects the organized turbulent flow behavior, based upon our experience from mean two-dimensional boundary layers. Large-scale coherent structures from the upstream boundary layer will be stretched around the protuberance. Depending upon the incident Reynolds number and the geometry of the protuberance, certain size or frequency structures may grow or be attenuated and a more narrow bandwidth spectrum may result. Experiments over a range of conditions are needed to determine when narrow band spectra occur.

Adverse pressure gradients on the downstream side of a protuberance or strut may cause the individual structures to move away from the corner and

agglomerate by pairing, since Shabaka and Bradshaw (Ref. 19) have noted that the mean flow vortex does wander from the corner under these conditions. Separation is likely, with rapidly growing large-scale structures supplying reversed flow, which also occurs in the mean two-dimensional separation case. In fact there are no detailed mean flow turbulence measurements available for this separated flow in the corner.

The flow downstream of the protuberance or strut is a three-dimensional turbulent boundary layer. If the downstream flow is subjected to an adverse pressure gradient as is often the case, the protuberance corner separation may not reattach, but instead the separation can spread laterally across the boundary layer. Even if the separated corner flow does reattach, this momentum and energy deficient region of the flow is more prone to detachment when subjected to an adverse pressure gradient downstream. In cases where these types of flow interact with another structural element downstream, the flow structure is clearly important in designing the structural element for optimal performance.

In the current research program, which began May 15, 1984, measurements are and will be made on turbulent boundary layers around protuberances or struts and downstream, including strong adverse pressure gradient and detached flow regions. Information on the temporal flow behavior will be obtained by means of spectral analysis and space-time correlations of surface pressure transducer and hot-wire anemometry. Time-averaged measurements of U, V, W, $\overline{-uv}$, $\overline{-uw}$, $\overline{u^2}$, $\overline{v^2}$ and $\overline{w^2}$ will be obtained in detail for the region around the strut and the downstream three-dimensional turbulent boundary layer, including zones of detached flow. Surface pressure spectra can be used to estimate sound pressure levels outside of the turbulent flow.

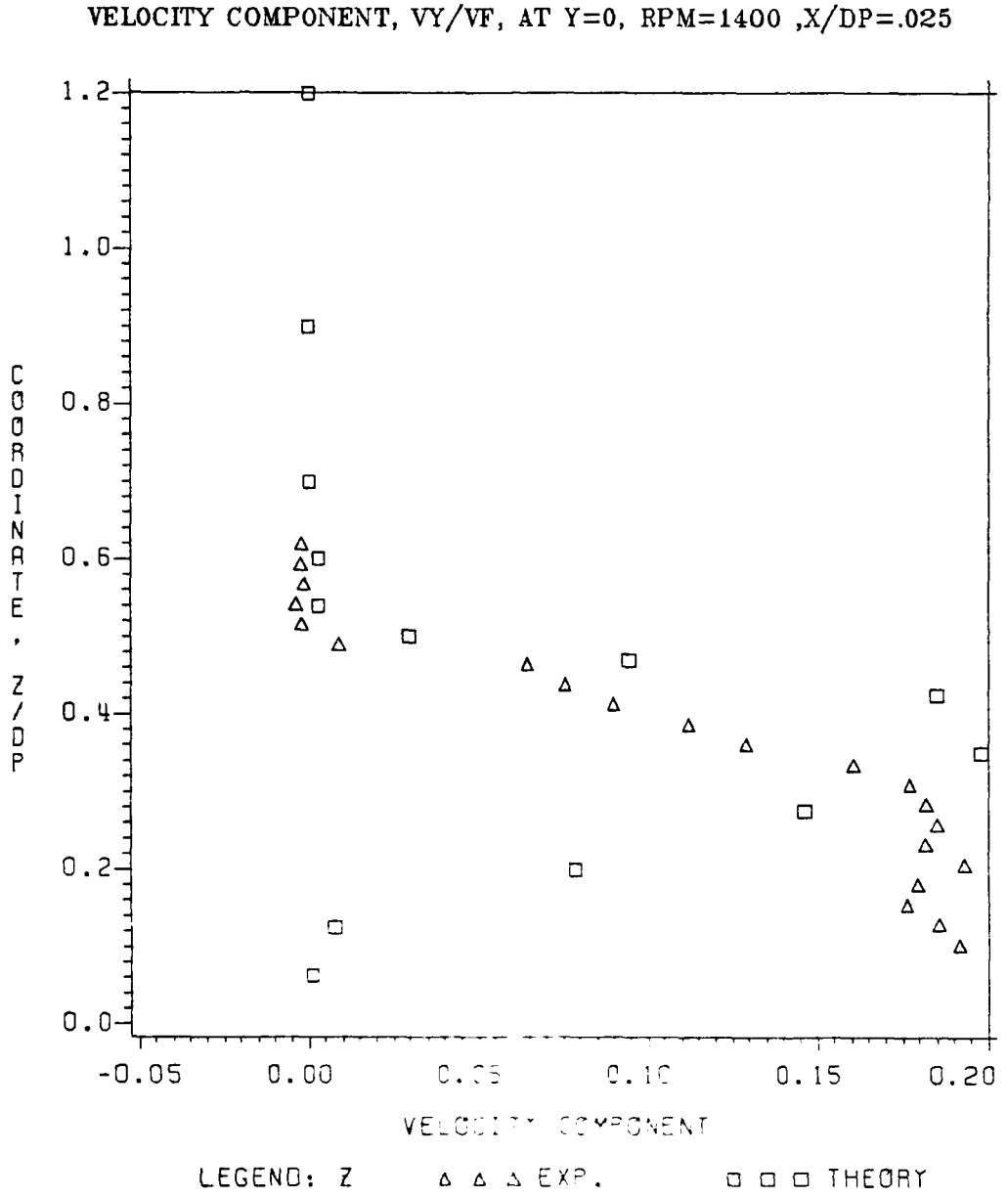

Figure 7. Swirl Velocity Profile Behind the Propeller at x/d=.025 for a Vertical Traverse.

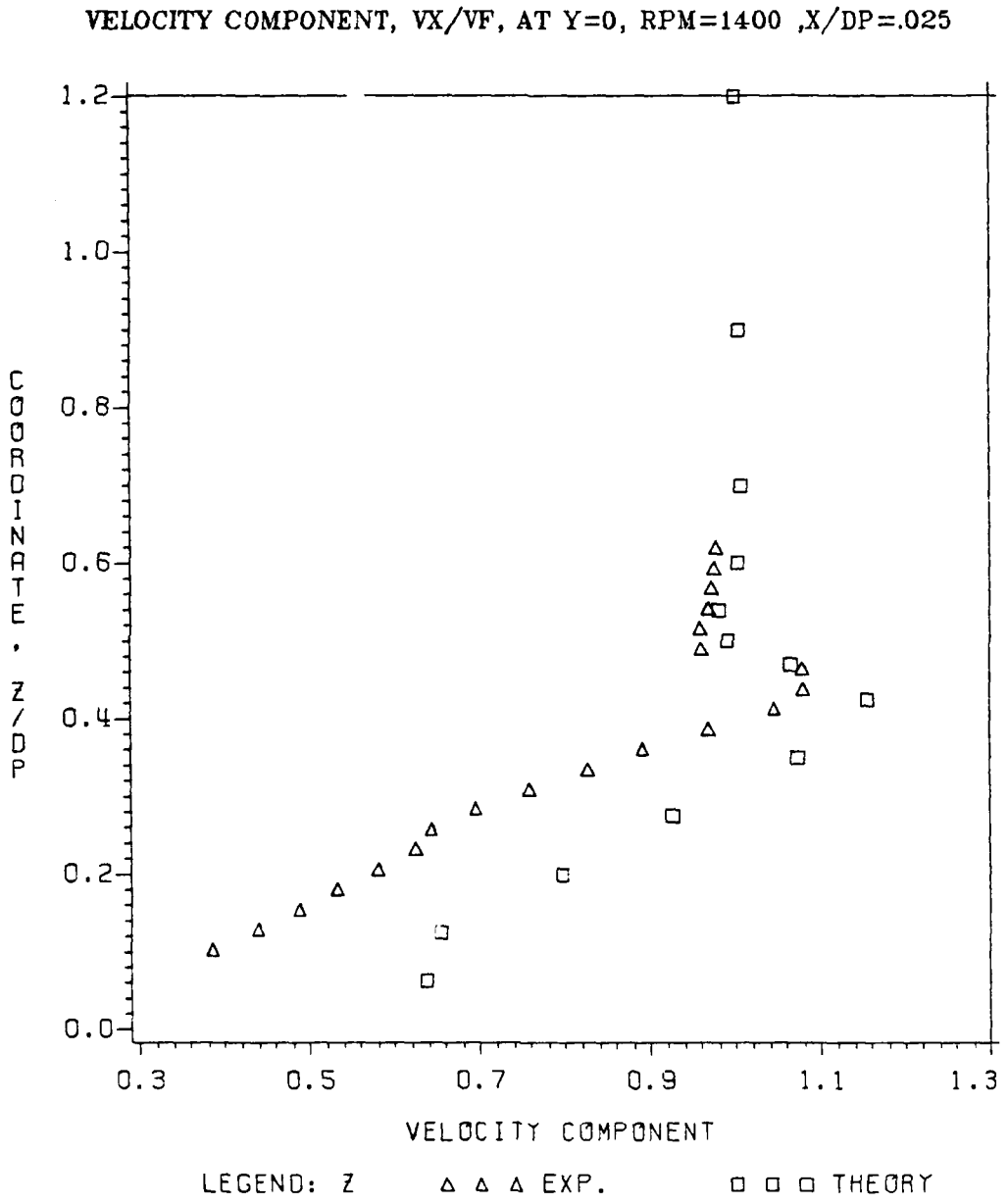

Figure 6. Axial Velocity Profile Behind the Propeller at x/d=.025 for a Vertical Traverse.

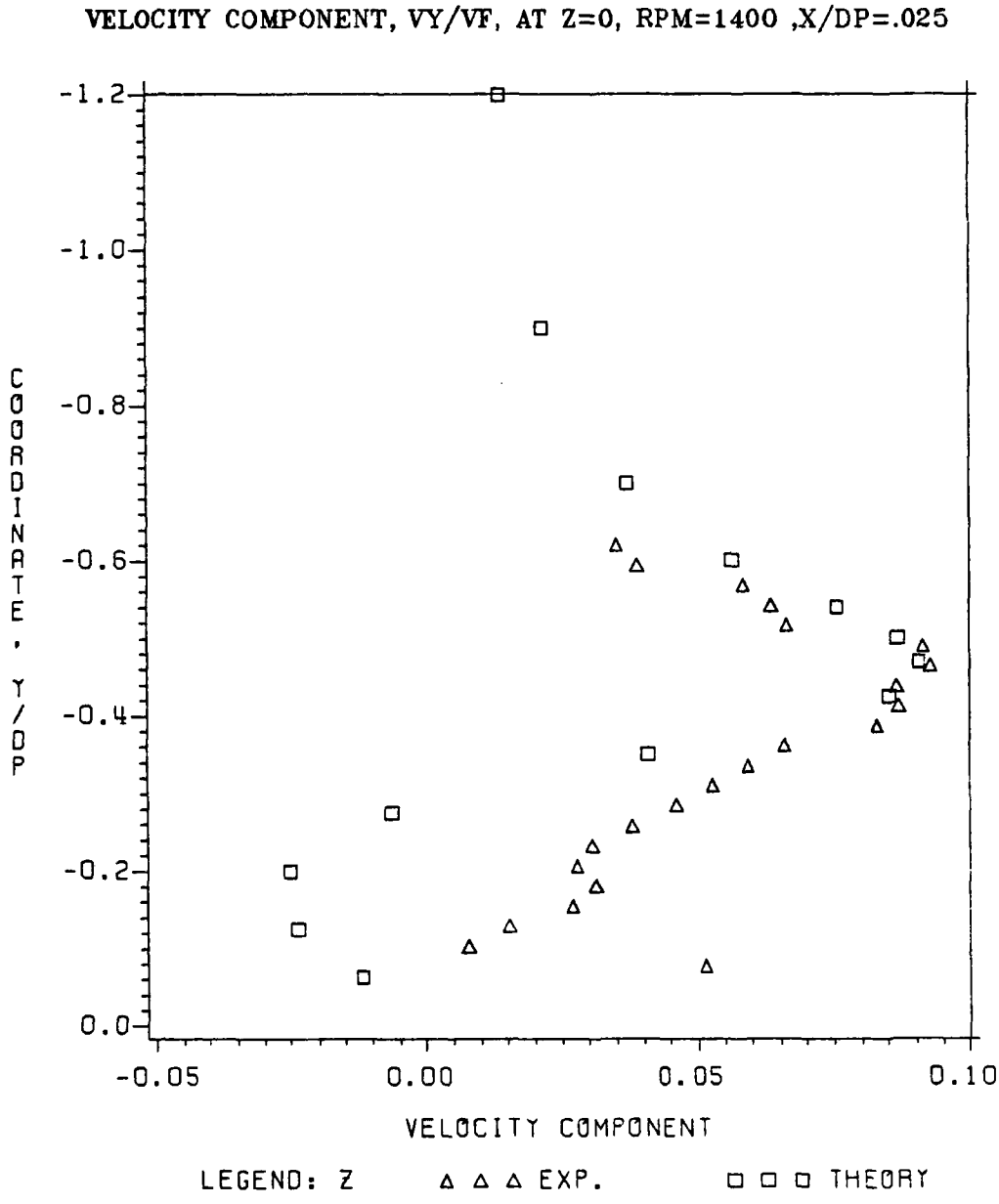

Figure 5. Radial Velocity Profile Behind the Propeller at x/d=.025 for a Horizontal Traverse.

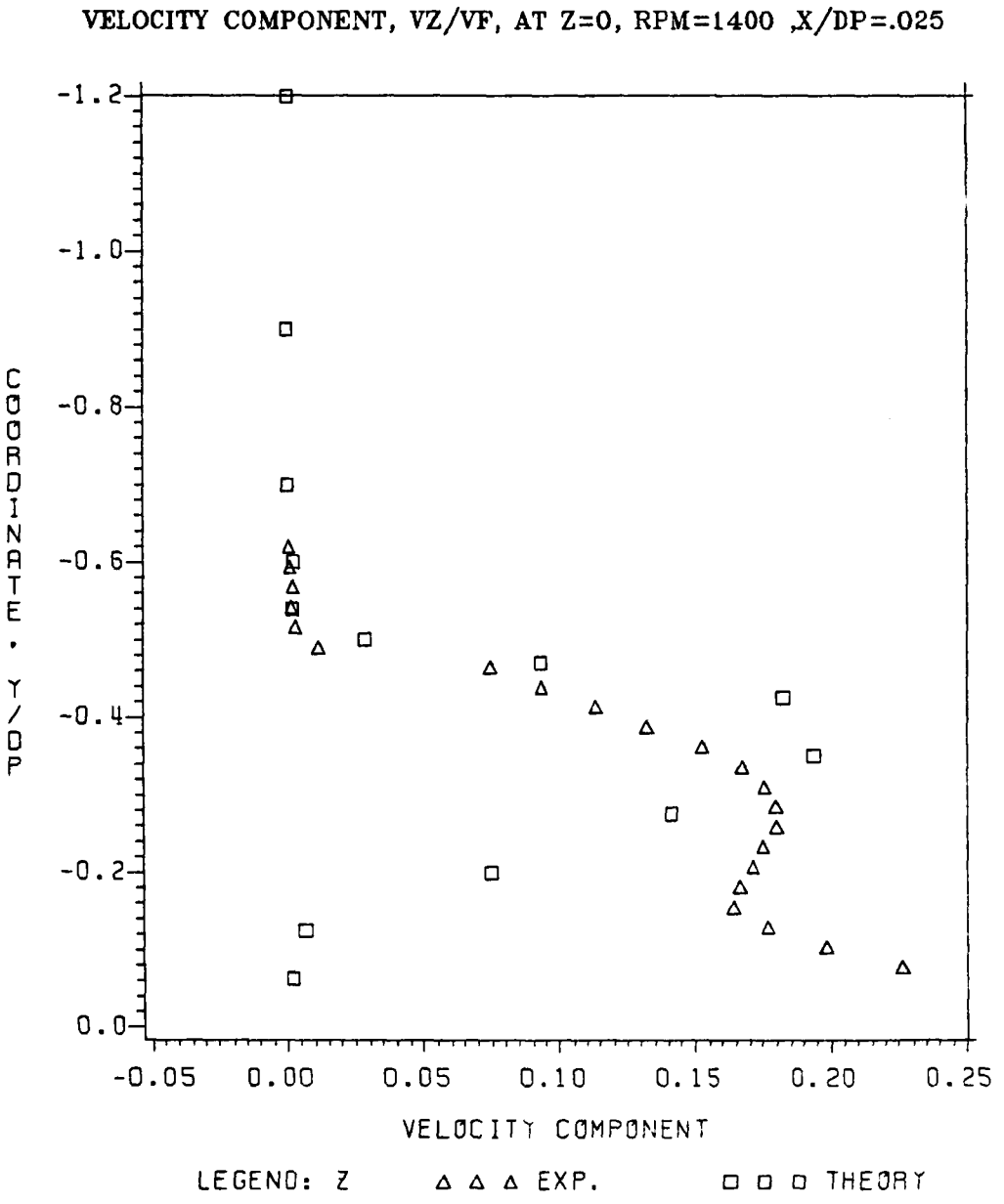

Figure 4. Swirl Velocity Profile Behind the Propeller at x/d=.025 for a Horizontal Traverse.

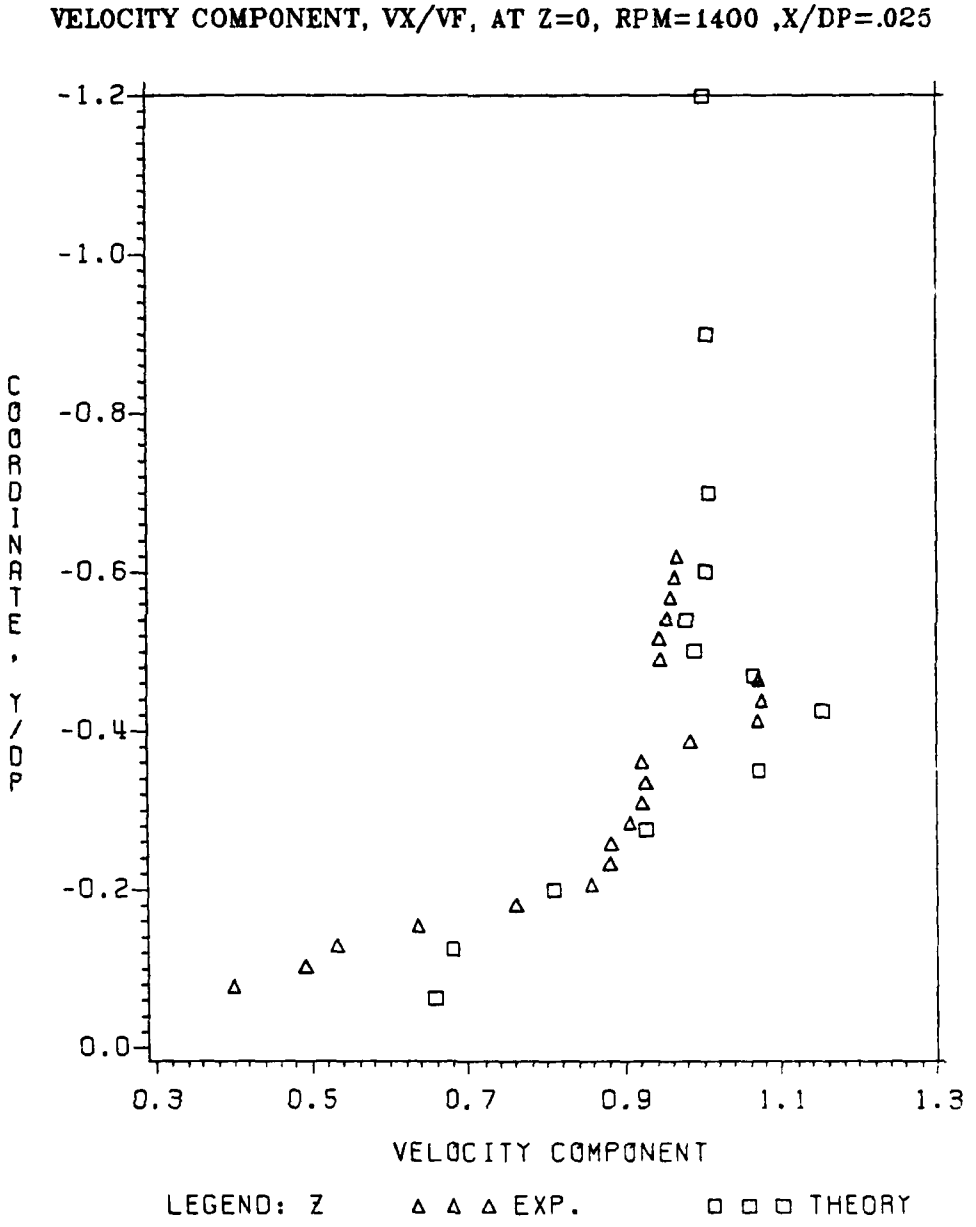

Figure 3. Axial Velocity Profile Behind the Propeller at x/d=.025 for a Horizontal Traverse.

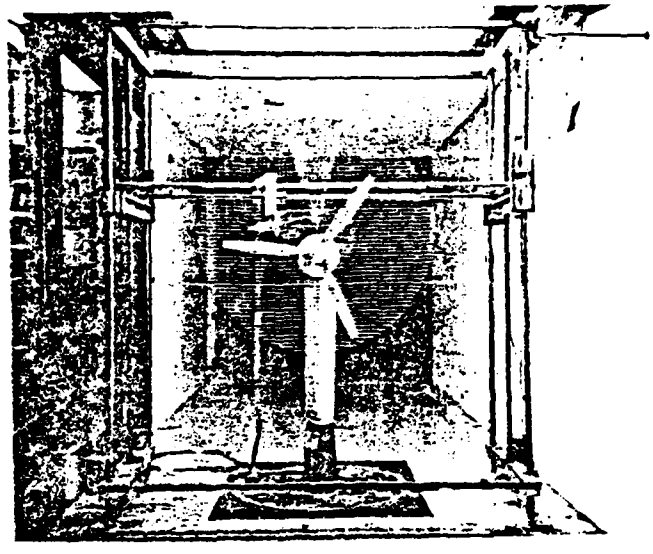

Figure 2. Front and Side Views of the Test Set Up in the Wind Tunnel.

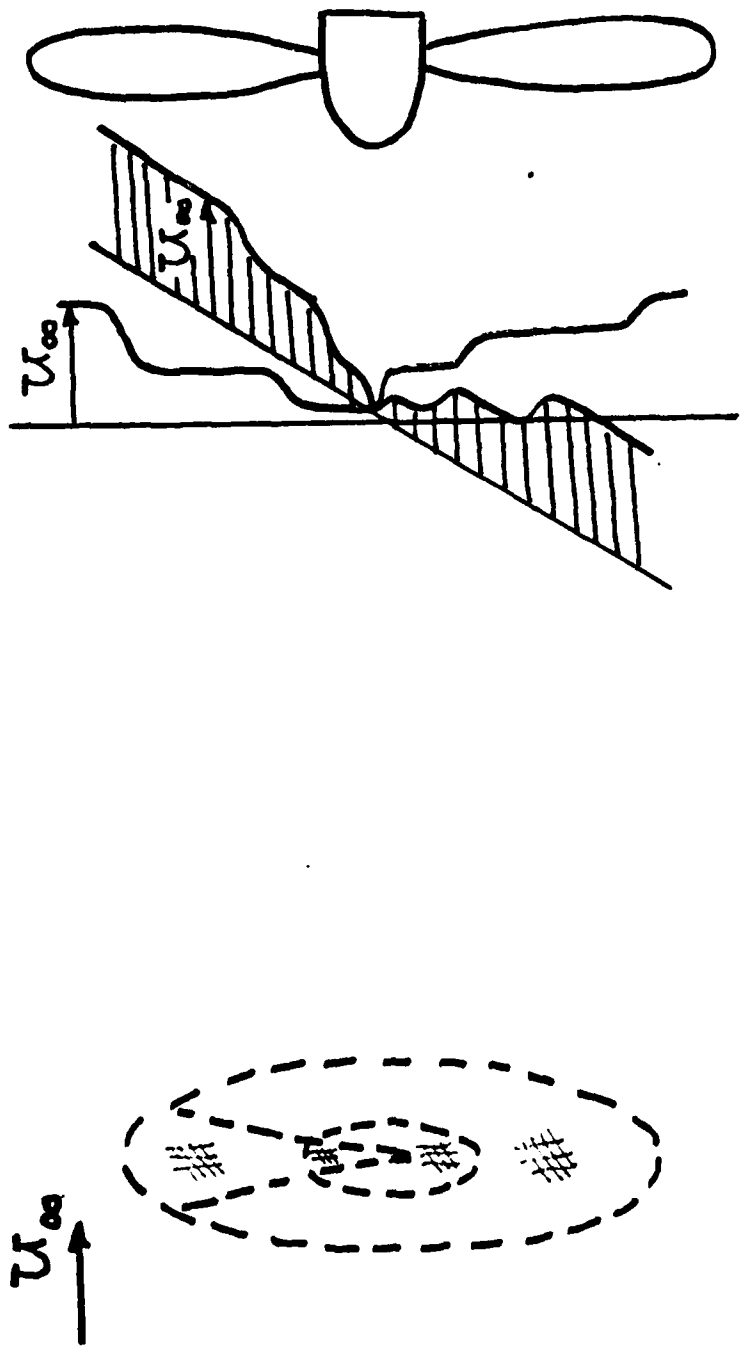

Figure 1. Schematic of the Analyzed Flow.

Figures

used to adjust the suction and jet flows to produce the desired streamline curvature and minimize blockage effects.

wire probes also show normal zero-pressure-gradient flow behavior without any preferred frequency (Ref. 24).

In work sponsored by NASA, McGrath and Simpson (Ref. 23) have obtained surface pressure spectra (Figures 14 and 15), pressure fluctuation wave speeds, and streamwise and spanwise coherence measurements. Figure 14 shows that the surface pressure spectra at lower frequencies agree with one another in terms of the outer region variables non-dimensionalizing variables U_e and the displacement thickness δ. Figure 15 shows that the higher frequency surface pressure fluctuation spectra correlate when non-dimensionalized on wall variables U_τ and ν/U_τ. No discrete preferred frequency has been observed in any of these surface pressure fluctuation data.

Figure 16 shows the shape of the cylindrical appendage that is currently being fabricated on a computer-controlled milling machine and will be used in the wind tunnel shown in Figure 17. The nose of this 12 inch chord protuberance is a 1.5 to 1.0 half ellipse while the tail portion beginning at the maximum thickness has the shape of a NACA 0020 airfoil. The 2.83 inches maximum thickness protuberance produces some blockage effects. In particular, the flow in the trailing portions of the corners of this junction will not be subjected to the same streamwise pressure gradients as in an infinite stream unless blockage effects are properly accounted for. The wall jet and suction boundary layer control system will be used to minimize blockage effects. As shown in Figure 18, inviscid flow streamlines for this body in an infinite stream show that there is some streamline curvature 18 inches from the body. The boundary layer wall jet and suction system will be used to suck off flow and produce this streamline curvature. Mean surface pressures calculated from potential flow will be

than 30 boundary layer thicknesses downstream of location A to insure that a normal two-dimensional zero-pressure-gradient boundary layer exists just upstream of the protuberance.

Downstream of the protuberance the flow will reattach to some degree. Downstream of location B the flow is subjected to a strong adverse pressure gradient that can be adjusted by the upper wall. The momentum deficient wake from the protuberance will be the first part of the flow to detach in a mean three-dimensional pattern. Judging from the results from mean two-dimensional flow the detached flow structure is dominated by the large-scale structures.

Figure 11 shows that upstream of the protuberance the classical U^+ vs. Y^+ "law-of-the-wall" velocity profile exists near the wall. The surface skin friction factor obeys the classical Ludwieg-Tillmann correlation (Ref. 22). The Reynolds shearing stress distributions across this boundary layer were obtained by cross-wire and triple-wire hot-wire anemometer probes (Ref. 24) and are in good agreement with earlier distributions for this type of flow (Figure 12). Measurements of $\overline{u^2}$ by single, cross-wire, and triple-wire hot-wire anemometers are in good agreement as discussed by Ahn (Ref. 22). Measurements of $\overline{v^2}$ by cross-wire and triple-wire probes agree away from the wall where triple-wire measurements are valid (Ref. 24). Measurements of $\overline{w^2}$ are in agreement with earlier turbulent boundary layer results.

Figure 13 shows that u fluctuation spectra from single hot-wire data have normal wideband features without any preferred single frequency (Ref. 22). This indicates no appreciable single frequency unsteadiness in this wind tunnel flow. Spectra for v, -uv and w obtained by cross and triple

3-D Turbulent Flows from Hull Appendage Junctions

During the first phase of this work, our goal is to determine the time-dependent features of protuberance flows for a range of practical conditions. Turbulence spectra, cross-spectra, and space-time correlations of hot-wire anemometer signals of u around the protuberance and downstream will be used to obtain this information. Hot-wire anemometer measurements upstream of the protuberance and downstream of reattachment will be made to document each condition.

During the past first year of this phase (May 15, 1984 through May 14, 1985), detailed turbulence measurements have been made of the zero-pressure gradient boundary layer that approaches the protuberance (Refs. 22, 23 and 24). The temporal structure of this type flow has been examined over a range of momentum thickness Reynolds numbers Re_θ between 2500 and 7000. Spanwise and streamwise space-time correlations and cross-spectral distributions of fluctuations, $\overline{u^2}$, $\overline{v^2}$, $\overline{w^2}$ and $\overline{-uv}$ Reynolds stresses, and surface pressure spectra have been obtained to thoroughly document the time-dependent behavior of zero-pressure gradient turbulent boundary layers approaching a protuberance. This is extremely important so that we can know if the time-dependent narrow frequency bandwidth motions observed by Rood are due to the upstream zero-pressure gradient boundary layer of due to the presence of the protuberance.

Figure 9 shows a sideview schematic of the 26 feet long, 3 feet wide wind tunnel test section used in these experiments. The flow enters from the left, forming a mean two-dimensional turbulent boundary layer on the flat floor of the test section. The upper wall position is adjusted to produce a zero pressure gradient boundary layer between locations A and B (Figure 10). A cylindrical protuberance of interest will be placed more

problem. We view the results as "preliminary", because they have only very recently been made and are still under study. We used a finite element grid with 12 peripheral planes which means that the pie-shaped mesh piece in Figure 1 occupied one whole element. It is likely that one or two extra peripheral planes should be added in that area. Work to that end is now underway. Despite these reservations, the results obtained to date to be shown below are really quite good, and we look for our final calculations to provide a truly excellent simulation of this complex flow.

In Figure 3, we show measurements and calculations for the axial velocity profile right behind the propeller (X/D = 0.025) along a radial line in the horizontal direction in Figure 1. For that cut, the flow will not have passed through the extra pie-shaped mesh segment before passing through the propeller. Figure 4 gives the swirling velocity component profile along the same radial cut, and Figure 5 shows the corresponding radial velocity. One can note the generally good agreement except near the hub and drive shaft ($Y/D \leq 0.2$).

Measurements and predictions along a vertical cut (see Figure 1), i.e. for flow that has passed through the extra wedge of mesh before entering the propeller, at X/D = 0.025 are shown in Figures 6, 7 and 8. The agreement is good but not so good as for the other radial cut. Again, we attribute this to a need for better element grid resolution in this sector.

PROGRESS REPORT

Numerical Solution of 3-D, Turbulent Propeller Flows

In the original (1983) plan, work for this year would have involved an axisymmetric, sharp-tailed, slender body ahead of the propeller. The approach flow was to be taken as three dimensional, i.e. varying with angle around the body, θ. This was called Problem #2. This represented a very large jump in complexity beyond Problem #1 - a propeller in a linear shear flow. Our experience with Problem #1 and consultations with DTNSRDC personnel indicated that the original Problem #2 should properly be split into two phases - Problems #2A and #2B. Problem #2A involves a peripherally varying inflow velocity profile similar to that expected in the original Problem #2 except that the solid body is removed. The desired inflow velocity distribution is generated by a wire mesh disk with radial and peripheral variations in mesh spacing (see Figure 1). This method is commonly used in propeller testing. Problem #2A was treated this year. Calculated results were compared to wind tunnel measurements using the same propeller as for Problem #1.

A photograph of the test apparatus in the wind tunnel is shown in Figure 2. We are using the same propeller as for our earlier work, but the test conditions are different. The freestream velocity is 44 ft/sec and the propeller is nominally "self-propelled" cancelling the drag of the screen disk. The rpm was 1400 giving $J = .96$. The propeller drive system and the thrust and torque measurements are improvements over our previous devices. We have measured both mean flow and turbulence quantities.

To this point, we have made complete, but preliminary, calculations using the basic methods described in Ref. (11) extended to this complex

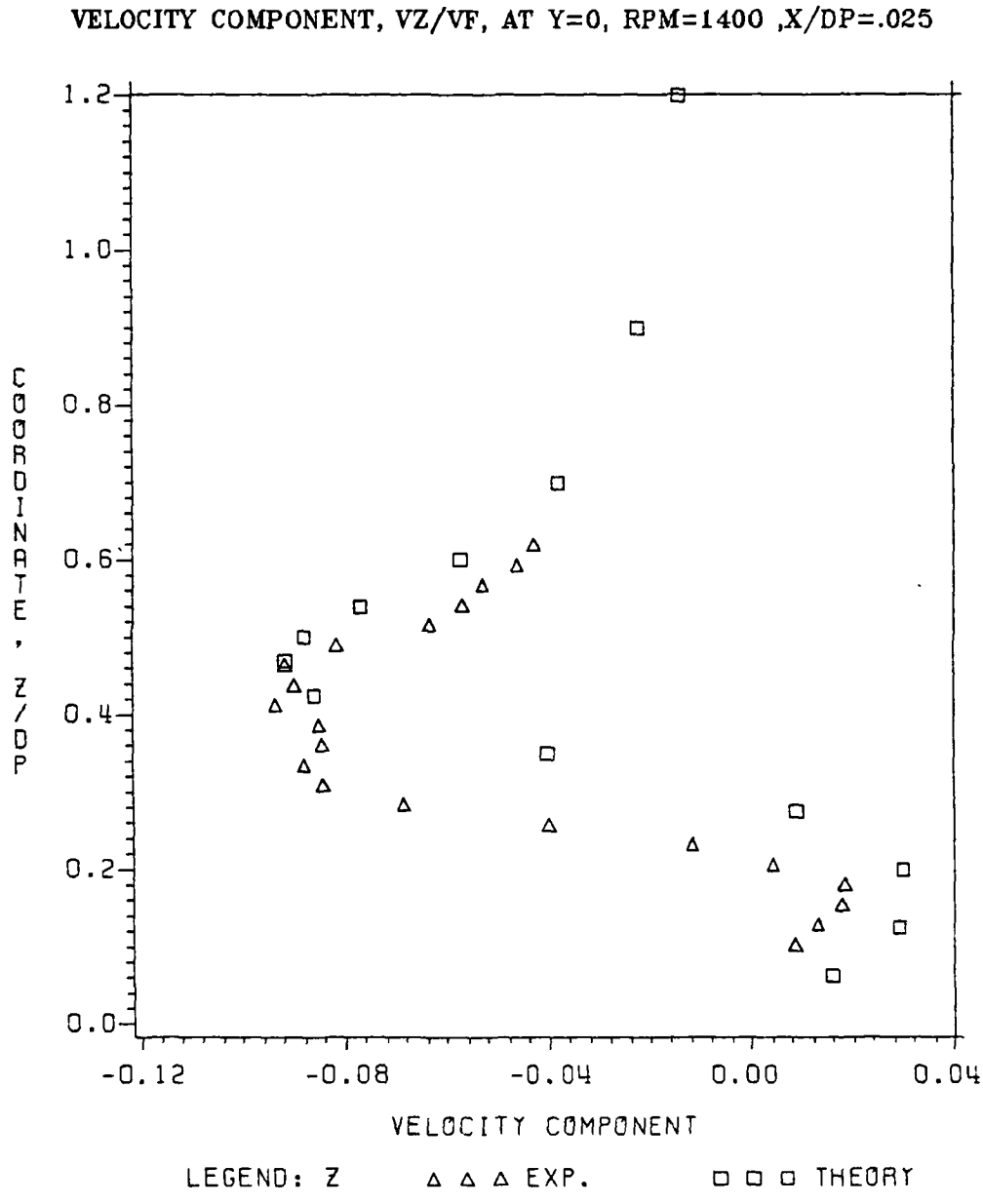

Figure 8. Radial Velocity Profile Behind the Propeller at x/d=.025 for a Vertical Traverse.

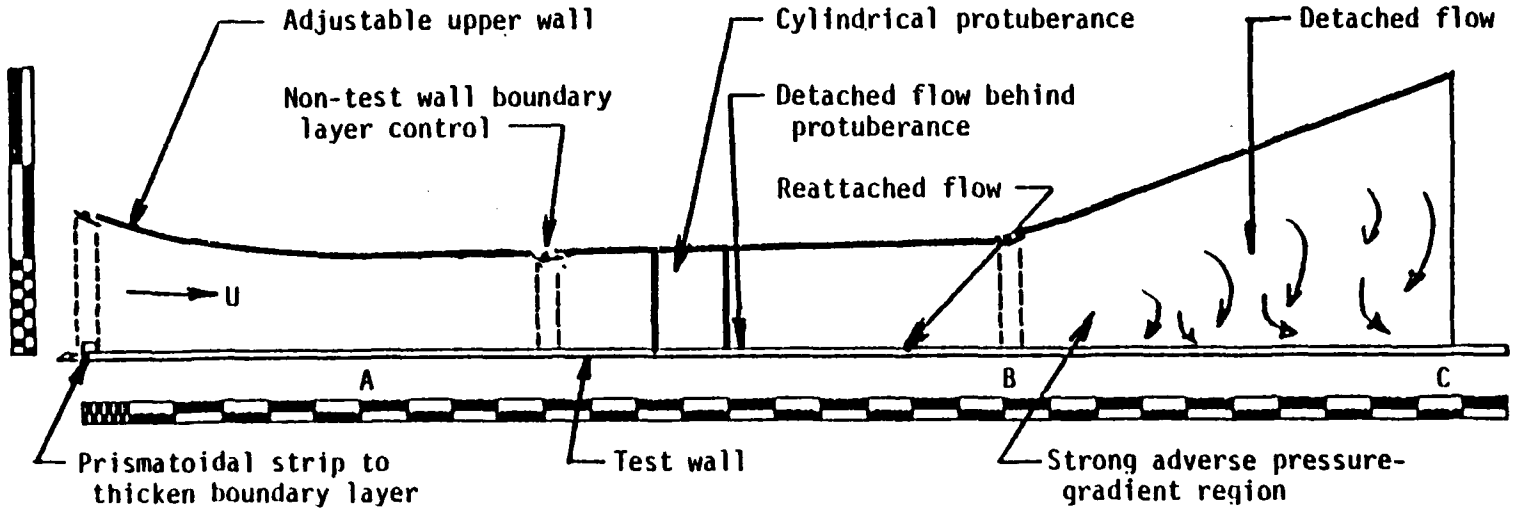

Figure 9. Sideview Schematic of the Wind Tunnel Test Section for the Protuberance-Hull Junction Flow. Major Divisions on Scales: 10 Inches.

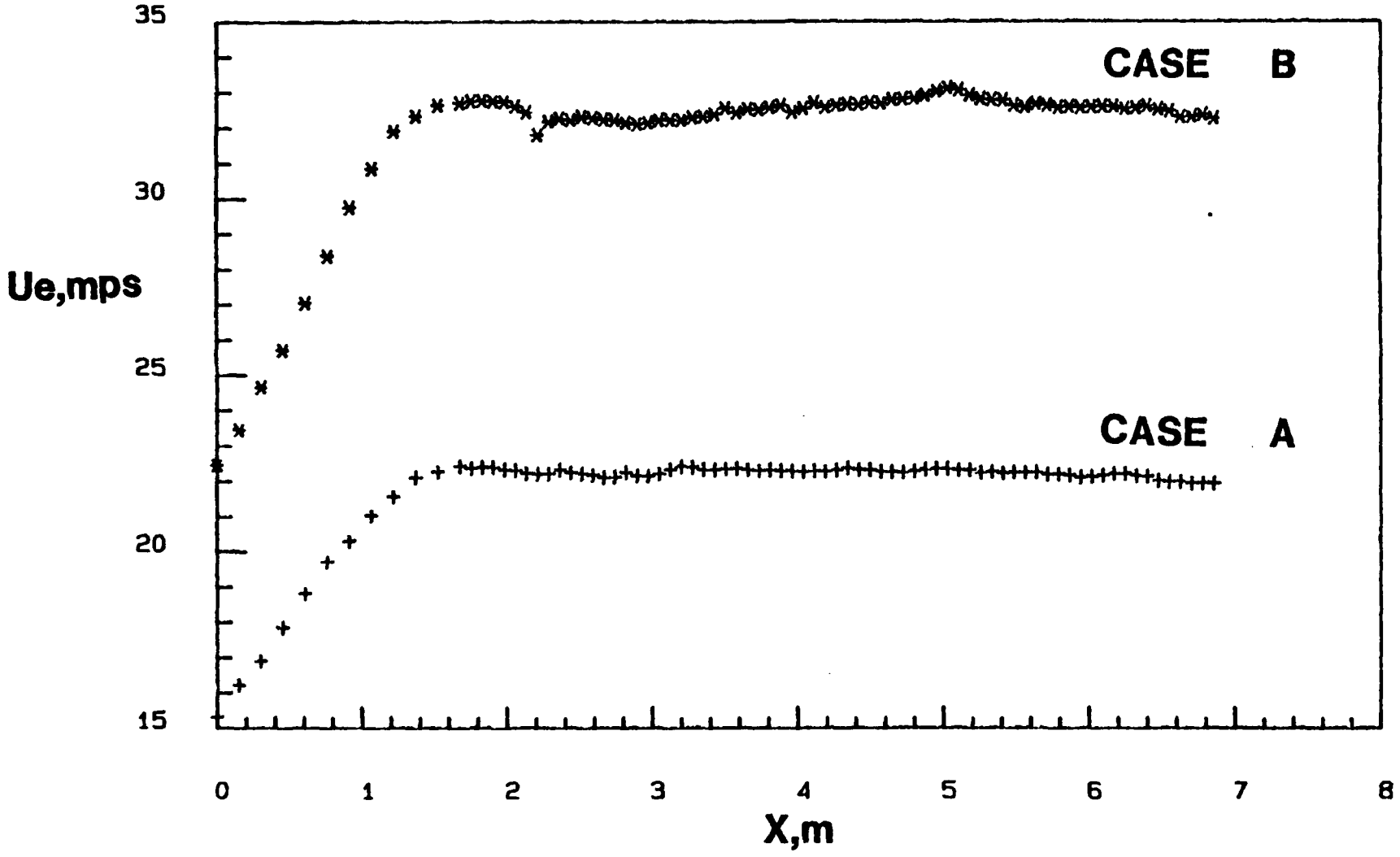

Figure 10. Freestream Velocity Distributions Along Wind Tunnel Test Section Centerline. Case A Used in Protuberance-Hull Junction Flow (Ref. 22).

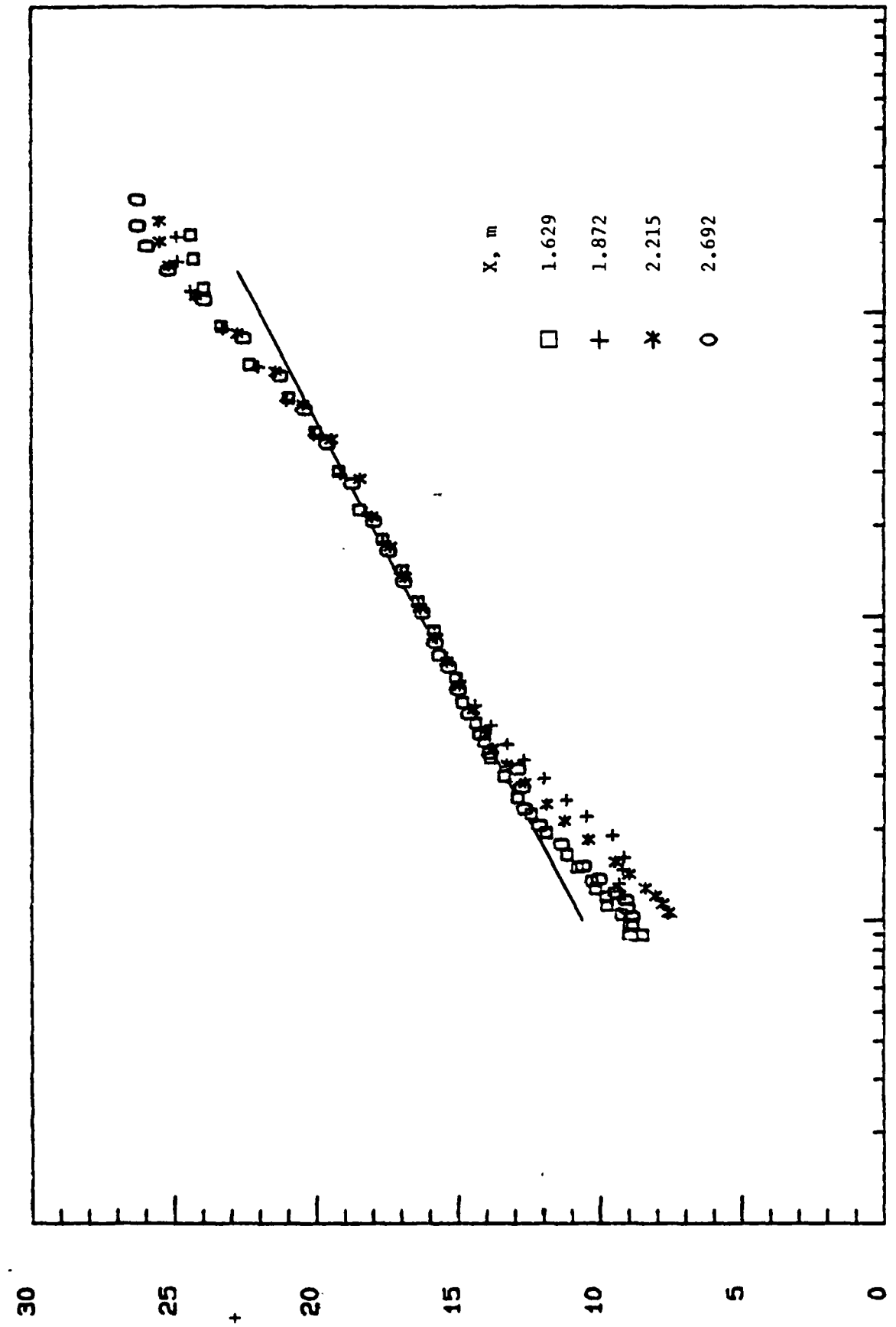

Figure 11. Classical "Law-of-the-Wall" Velocity Profile Flow the Zero-Pressure-Gradient Turbulent Boundary Layer (Case A) Upstream of the Appendage (Ref. 22).

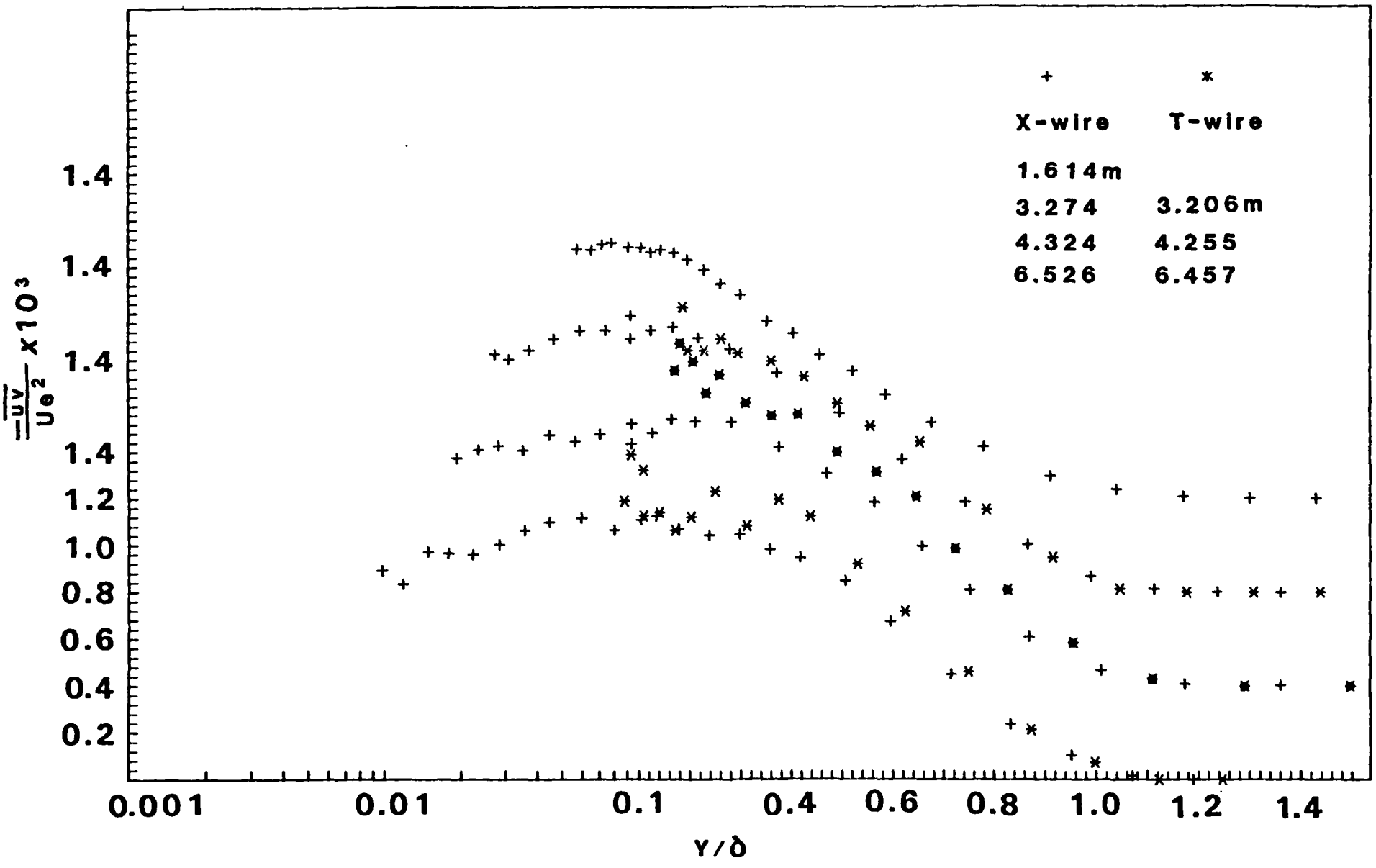

Figure 12. Reynolds Shearing Stress $-\overline{uv}/U_e^2$ vs. Y/δ Profiles from Cross-Wire and Triple-Wire Anemometers along the Test Section Floor for Case A. Increasing Streamwise Locations from Top to Bottom of Figure. Note Displaced Ordinates. Solid Symbols for Triple-Wire Results at 4.255 m. (Ref. 24)

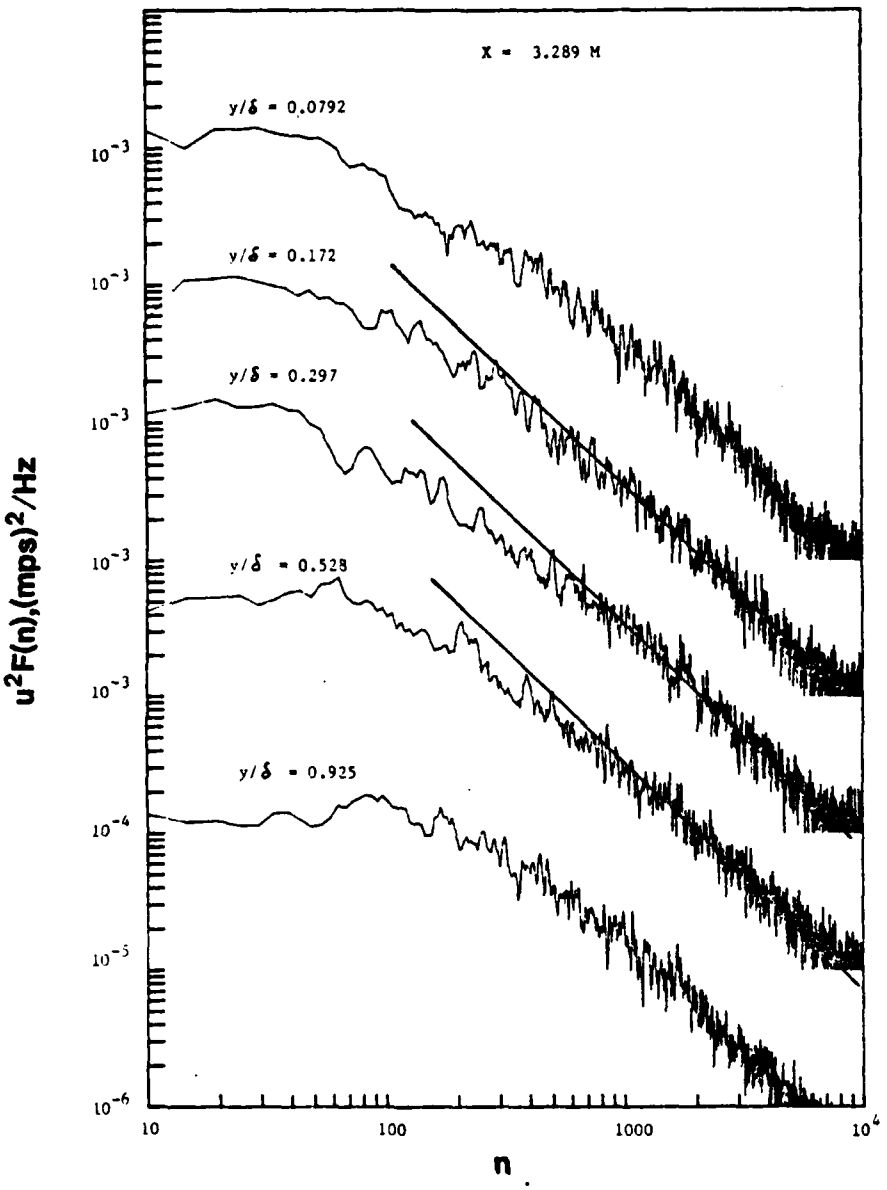

Figure 13. Streamwise Velocity Fluctuation Spectra at X = 3.289 m for Various Y/δ Positions within the Case A Zero-Pressure-Gradient Boundary Layer. Solid Straight Lines Denote $n^{-5/3}$ Inertia Subrange for These Spectra.

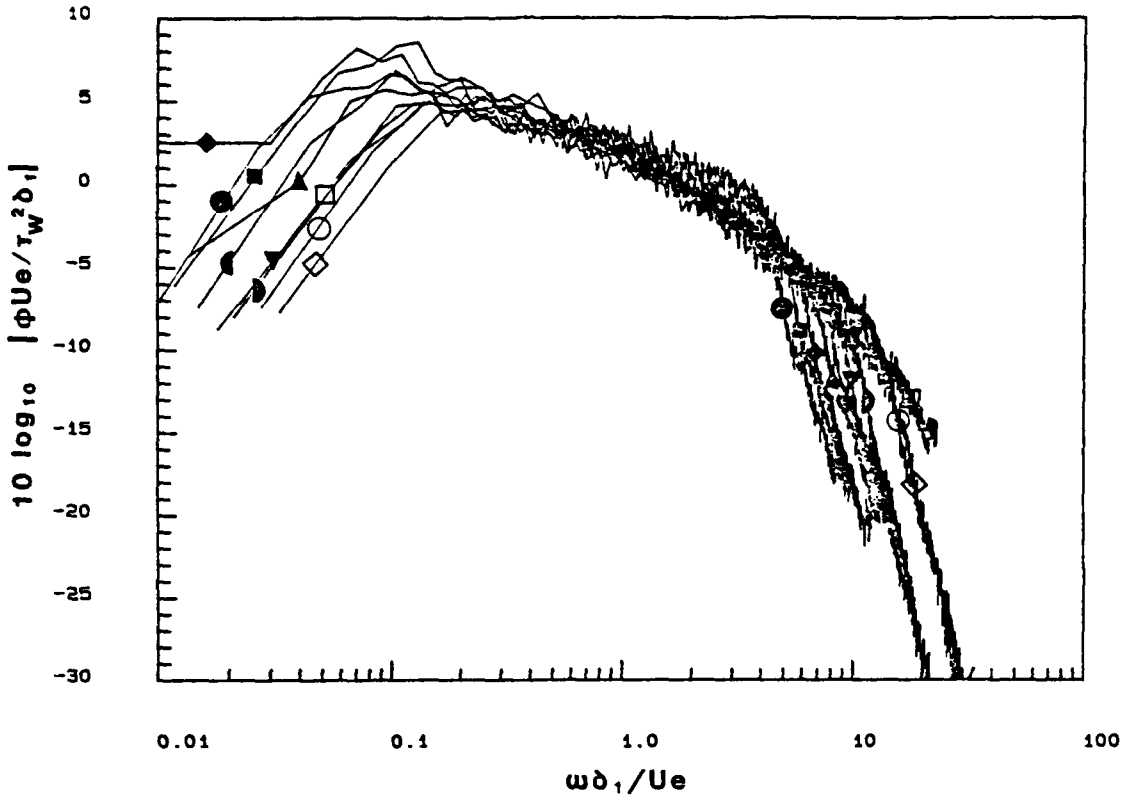

Figure 14. Surface Pressure Spectra in Outer Region Non-Dimensional Variables for the Case A Zero-Pressure-Gradient Turbulent Boundary Layer Along the Test Section Floor. Note Good Agreement Among Data for $0.1 < \omega\delta_1/U_e < 1$ (Ref. 23).

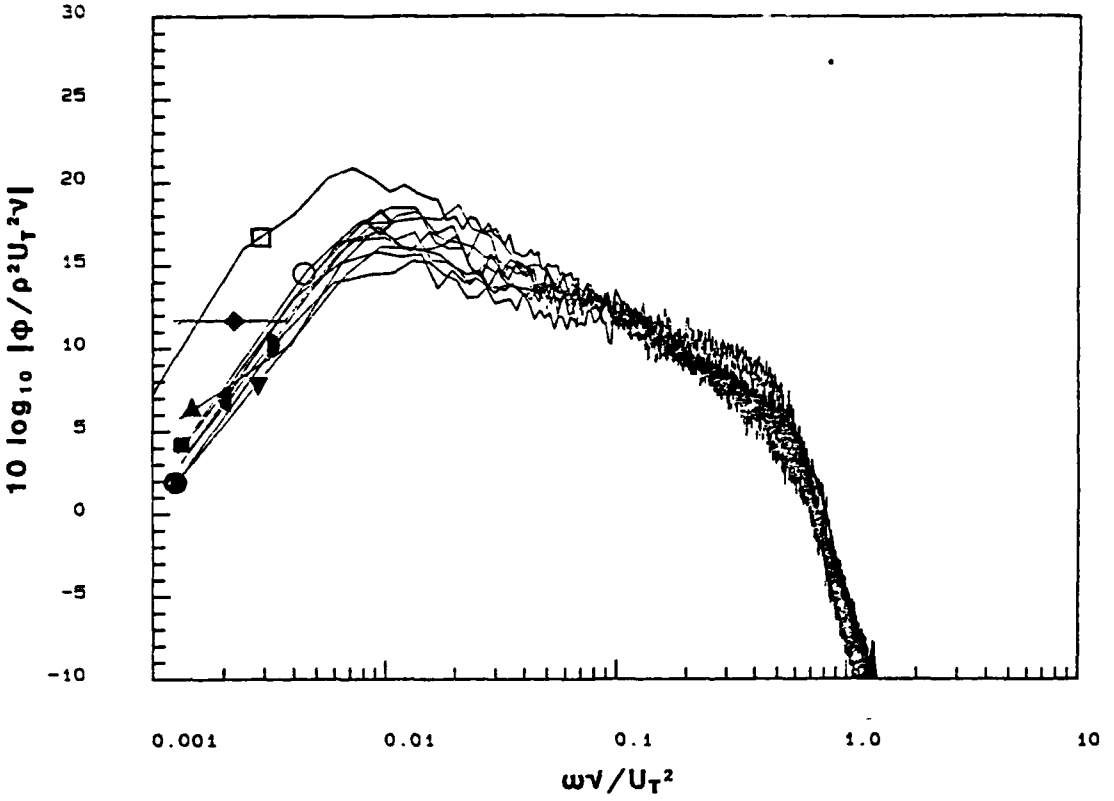

Figure 15. Surface Pressure Spectra in Wall Region Non-Dimensional Variables for the Case A Zero-Pressure-Gradient Turbulent Boundary Layer Along the Test Section Floor. Note Good Agreement Among Data for $\omega\nu/U_e^2 > 0.1$ (Ref. 23).

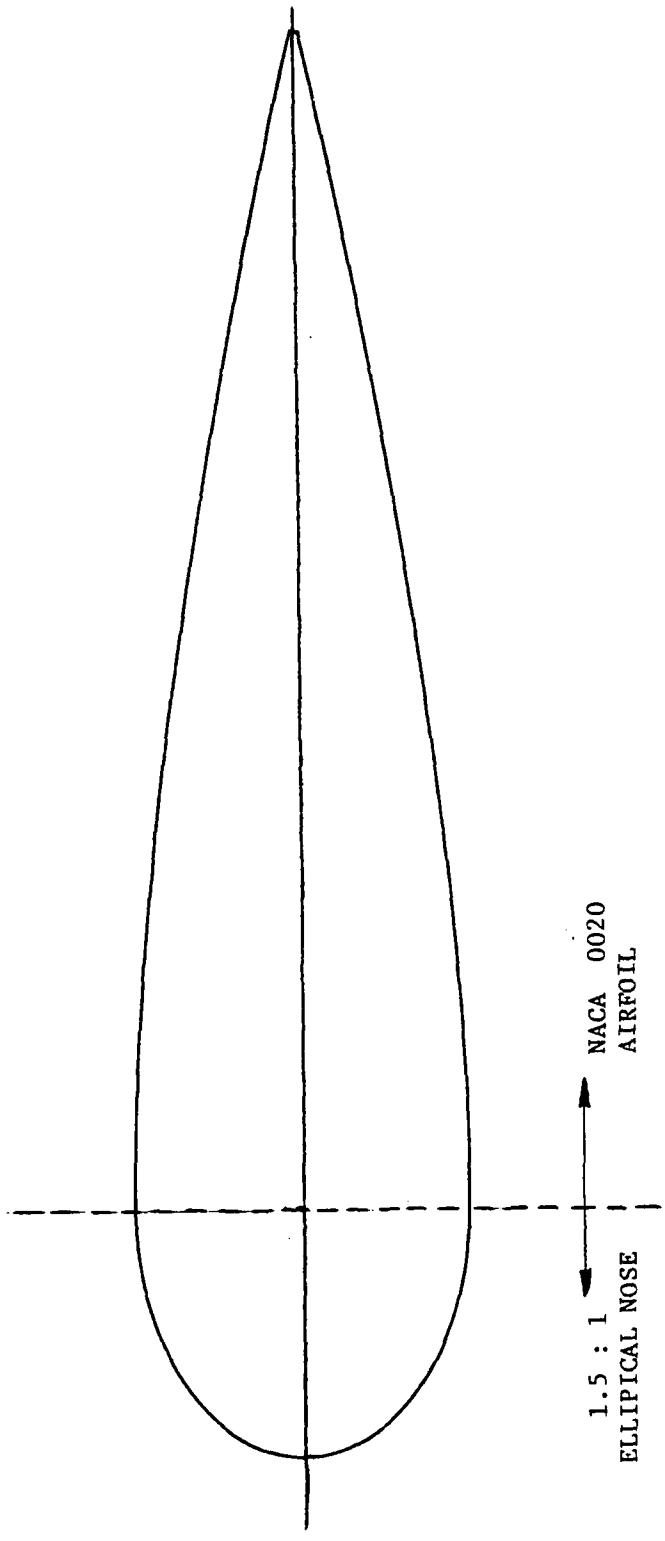

Figure 16. Body Shape of the 12 Inches Chord Cylindrical Appendage To Be Used in the Protuberance-Hull Junction Flow Experiments. Nose is 1.5:1 Ellipse While Trailing Portion from Maximum Thickness is NACA 0020 Airfoil Shape.

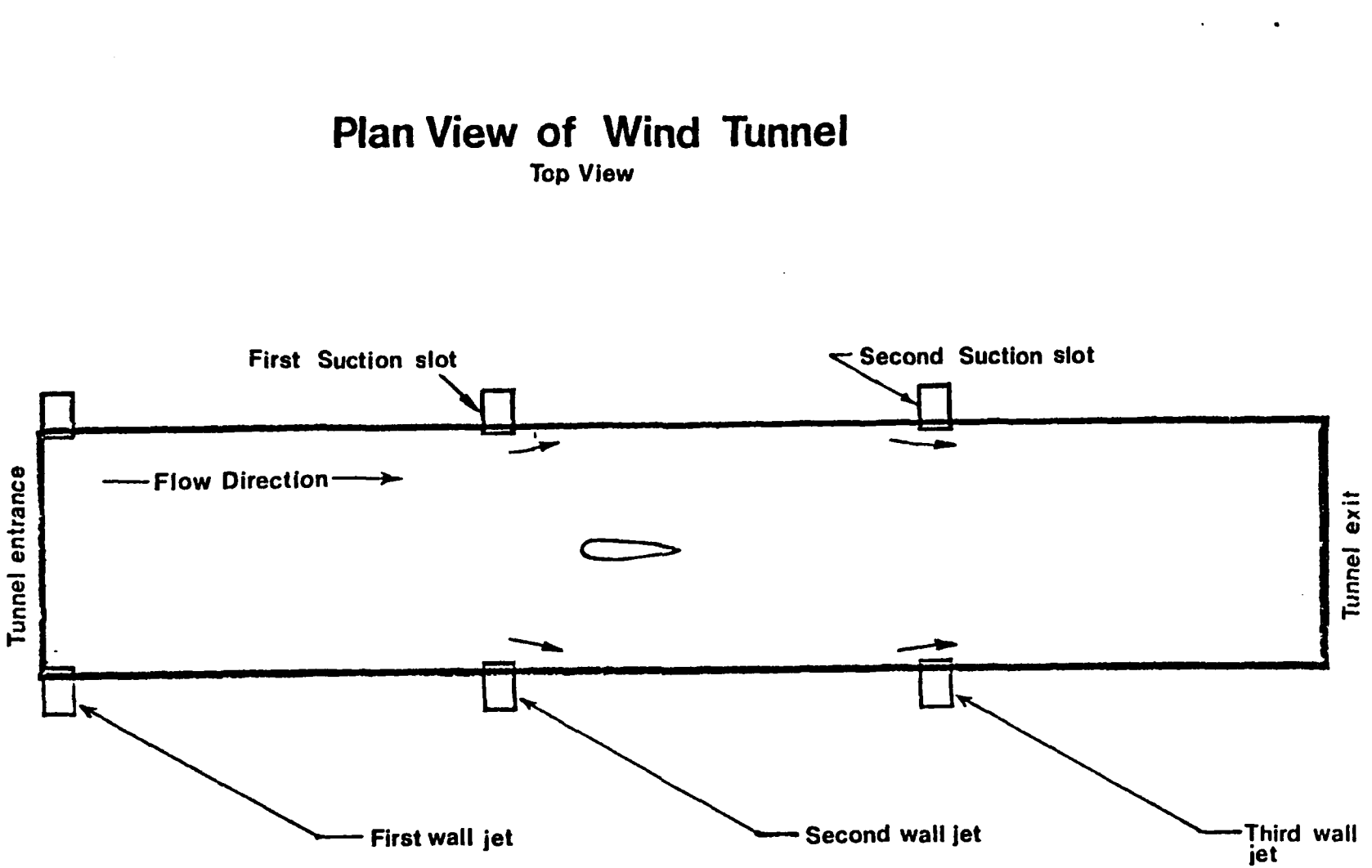

Figure 17. Plan View of Wind Tunnel Test Section Showing Side Wall Jet and Suction Boundary Layer Control Slots for Reducing Blockage Effects of Appendage.

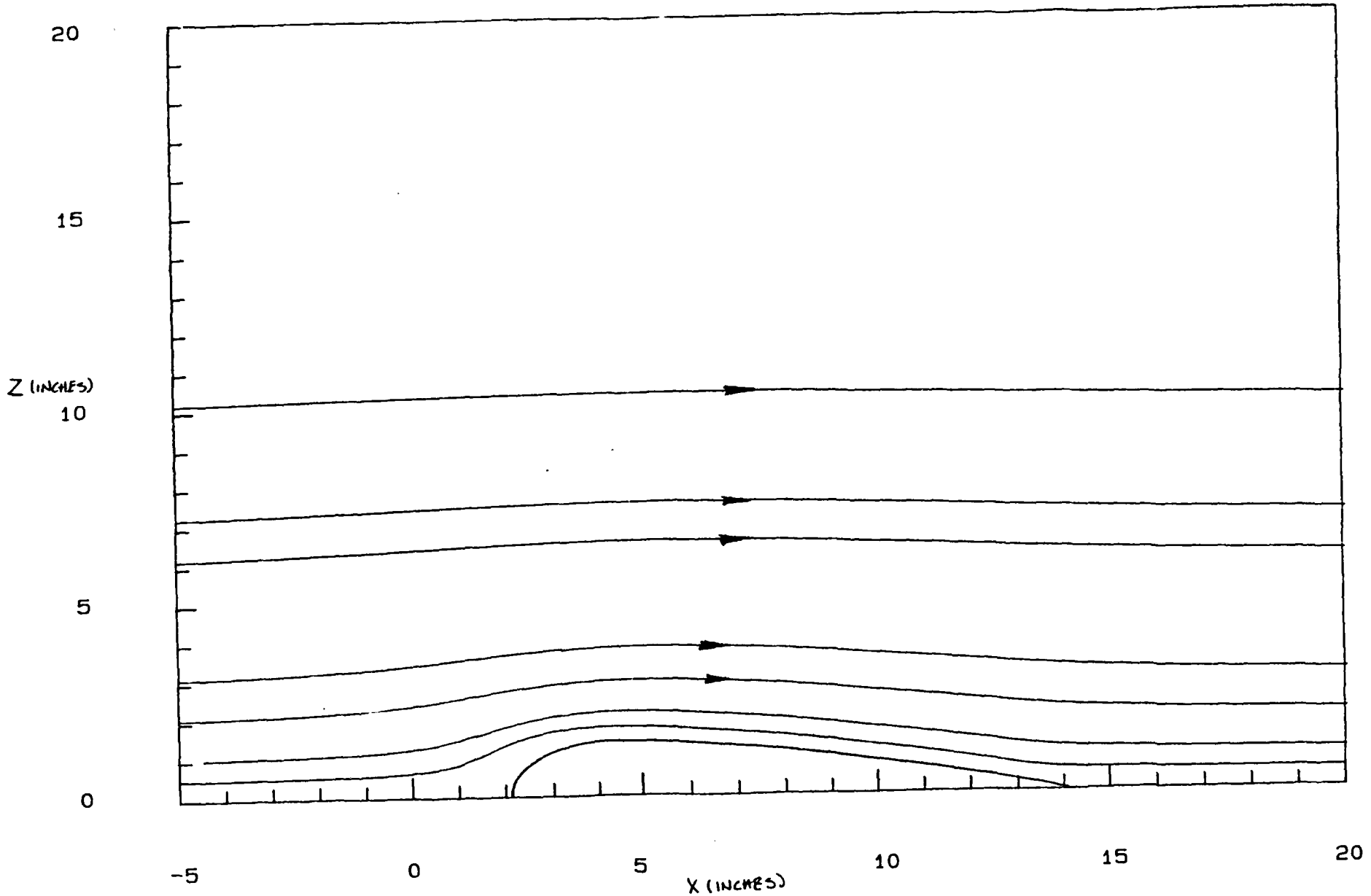

Figure 18. Inviscid Flow Streamlines for the Two-Dimensional Body Shown in Figure 16 When Submerged in an Infinite Stream. Abscissa Represents Centerline of Body and Line of Symmetry for the Flow. Side Wall Boundary Layer Control System Will Be Adjusted to Produce Such Streamlines by Maintaining Inviscid Mean Pressure Distribution in Streamwise Direction Along Z = ±10 Inches Line.

REFERENCES

1. Sparenberg, J.A., "On the Potential Theory of the Interaction of an Acutator Disk and a Body," Journal of Ship Research, December 1972.

2. Sparenberg, J.A., "On the Linear Theory of an Actuator Disk in a Viscous Fluid," Journal of Ship Research, March 1974.

3. Kim, K-H. and Kobayoshi, S., "Pressure Distribution on Propeller Blade Surface Using Numerical Lifting Line Theory," SNAME Propellers '84 Meeting, May 1984.

4. Huang, T. et al., "Propeller/Stern/Boundary-Layer Interaction on Axisymmetric Bodies," DTNSRDC Rept. 76-0113, December 1976.

5. Cox, B.D. and Hansen, A.G., "A method for Predicting Thrust Deduction using Propeller Lifting Surface Theory," DTNSRDC Rept. 77-0087, November 1977.

6. Schetz, J.A. and Favin, S., "Numerical Solution for the Near Wake of a Body with Propeller," Journal of Hydronautics, Vol. 11, No. 4, October 1977, pp. 136-141.

7. Schetz, J.A. and Favin, S., "Numerical Solution of a Body-Propeller Combination Flow Including Swirl and Comparisons with Data," J. of Hydronautics, Vol. 13, No. 2, pp. 46-51, April 1979.

8. Bercovier, M. and Engelman, M.S., "A Finite Element for Incompressible Fluid Flows," J. Comp. Physics, 30, 181 (1979).

9. Engelman, M.S., Sani, R.L. and Gresho, P.M., "The Implementation of Normal and Tangential Velocity Boundary Conditions in Finite Element Codes for Incompressible Fluid Flow," to appear Int. J. Num. Meth. Fluids, 1981.

10. Engelman, M.S., Strang, G. and Bathe, K.J., "The Application of Quasi-Newton Methods in Fluid Mechanics," Int. J. Num. Meth. Eng., 1983.

11. Pelletier, D. and Schetz, J.A., "A Navier-Stokes Calculation of 3D Turbulent Flow Near a Propeller in a Shear Flow," AIAA Paper 85-0365, January 1985.

12. Dean, R. "Turbulent Secondary Flow of the First Kind," see Kline et. al. (1981), pp. 139-154, 1980.

13. Humphreys, D.A. and vandenBerg, B., "Three-Dimensional Turbulent Boundary Layers," see Kline et al. (1980), pp. 162-169, 1980.

14. Kline, S.J., Cantwell, D.J. and Lilley, G.M., ed., The 1980-1981 AFOSR-HTTM-Stanford Conferences on Complex Turbulent Flows: Comparison of Computation and Experiment, Vol. 1, 2 and 3, Stanford University Dept. Mechanical Engineering, 1981.

15. Shabaka, I.M.M.A., "Turbulent Flow in an Idealized Wing-Body Junction," Ph.D. Dissertation, Imperial College of Science and Technology, London, 1979.

16. Dechow, R., Dissertation University Karlsruhe, see Dechow, R. and Felsch, K.O., Turb. Shear Flows Sym. (1977), pp. 9.11-9.20, Pa. State Univ. (1977).

17. Mcallister, J.E., Pierce, F.J. and Tennant, M.H., "Direct Force Wall Shear Stress Measurement in Pressure-Driven Three-Dimensional Turbulent Boundary Layers," J. Fluids Engrg., 104, pp. 150-155, 1982.

18. Rubel, A., "Computational Technique for the Calculation of Inviscid Rotational Jet Impingement," AIAA Paper 78-1212, 1978.

19. Shabaka, I.M.M.A. and Bradshaw, P., "Turbulent Flow Measurements in an Idealized Wing/Body Junction," AIAA Journal, 19, pp. 131-132, 1981.

20. Barber, T.J., "An Investigation of Strut-Wall Intersection Losses," J. Aircraft, 15, pp. 576-681, 1978.

21. Oguz, E.A., "An Experimental Investigation of the Turbulent Flow in the Junction of a Flat Plate and a Body of Constant Thickness," Ph.D. Dissertation, Georgia Inst. Tech., 1981.

22. Ahn, S., "Measurements in Turbulent Boundary Layers," M.S. Thesis, Dept. Aerospace and Ocean Engrg., VPI&SU, in progress, 1985.

23. McGrath, B., "Some Features of Surface Pressure Fluctuations in Zero and Favorable Pressure Gradients," M.S. thesis, Dept. Aerospace and Ocean Engrg., VPI&SU, in progress, 1985.

24. Chew, Y.-T. and Simpson, R.L., "A Simple Data Reduction Method for Triple Sensors Hot-Wire Anemometers in Three-Dimensional Flow," manuscript in preparation, 1985.

PUBLICATIONS

1. Pelletier, D. and Schetz, J.A., "A Navier-Stokes Calculation of 3D Turbulent Flow Near a Propeller in a Shear Flow," AIAA Paper 85-0365, January 1985.

2. Pelletier, D. and Schetz, J.A., "A Turbulence Model for Finite Element Simulation of 3-D Turbulent Flows Near Propellers and Windmills," Fourth Int. Conf. Numerical Methods in Laminar and Turbulent Flow, Swansea, Wales, July 1985.

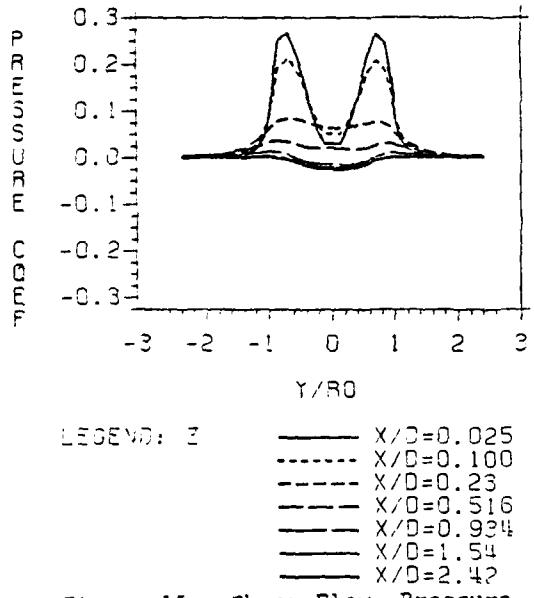

Figure 15: Shear Flow: Pressure Profiles

CONCLUSIONS

This work has developed a general-purpose, advanced computational technique for three-dimensional turbulent free shear flows past propellers. The main results can be summarized as:

1. predictions for uniform and shear flows past a propeller show excellent agreement with the experiments for the axial and swirl component of the velocity,

2. the simple turbulence model produced very accurate swirl predictions for both the uniform and shear flow cases. All previous numerical work on such flows provided poor predictions of the swirl,

3. the pressure predictions presented here for viscous turbulent flows through a propeller are the first known to the authors.

4. the numerical simulations show that the propeller exerts a strong upstream influence on the axial and radial velocity fields, and on the pressure field. There is negligible swirl upstream of the propeller,

5. the resulting Galerkin finite element algorithm is robust and stable, mostly due to the full coupling of the three momentum equations and the continuity equation. It captured the complex features of the shear flow. No gradual introduction of the thrust and torque as the iteration proceeds is required as opposed to previous work.

REFERENCES

1. Von Karman T. and Burgers J. M., "General Aerodynamic Theory - Perfect Fluids," Aerodynamic Theory, Vol. 2, W. F. Durand ed., California Institute of Technology, 1934.

2. Sparenberg J. A., "On the Potential Theory of the Interaction of an Actuator Disk and a Body," Journal of Ship Research, December 1972.

3. Sparenberg J. A., "On the Linear theory of an Actuator Disk in a Viscous Flow," Journal of Ship Research, March 1974

4. Schetz J. A. and Favin S., "Numerical Solution for the Near Wake of a Body with Propeller," Journal of Hydronautics, Vol. 11, No. 4, October 1977.

5. Schetz J. A. and Favin S., "Numerical Solution of a Body-Propeller Combination Flow Including Swirl and Comparison with Data," Journal of Hydronautics, Vol. 13, No. 2, April 1979.

peller on the pressure field is illustrated in Figure (10). The sudden, almost discontinuous, pressure increase, characteristic of actuator disks, is evident. Figure (11) shows that there is negligible swirl upstream of the propeller as predicted by vortex theory. The jump in the swirl across the propeller is a behavior akin to the shock wave in compressible flows. The small wiggles upstream of the propeller are typical of the use of Galerkin and central difference schemes for problems with sharp fronts. The near perfect axial symmetry of the swirl distribution is observed. The slipstream contraction is clearly seen in Figure (12)

Figure (13) presents axial velocity profiles along the y axis at various stations downstream of the propeller. The streamwise acceleration of the fluid downstream of the propeller due to pressure relaxation can be seen. The kinks near the tip of the propeller in the first two profiles of Figure (13) are characteristic of flows past propellers Ref.[16]. The asymmetries due to the shear in the approach flow can be seen most clearly in the shape of the peaks of axial velocity. The swirl profiles

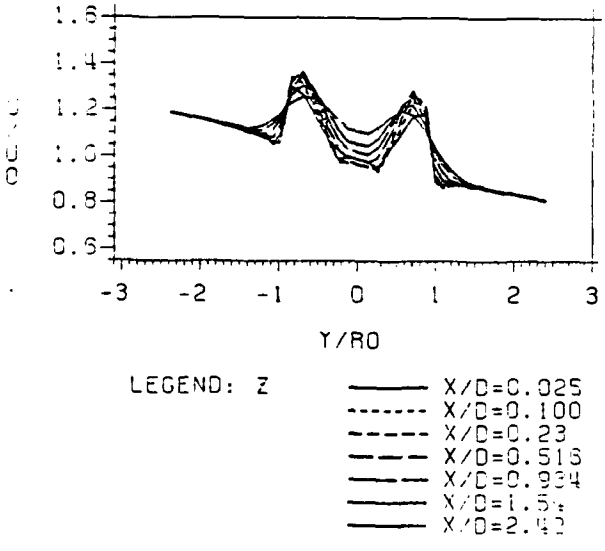

Figure 13: Shear Flow: Axial Velocity Profiles

at various axial stations are shown in Figure (14). The swirl level decays very slowly. The radial turbulent diffusion of momentum, characterized by flatter and wider profiles, is clearly seen . Pressure profiles are plotted in Figure (15) illustrating the decay downstream of the propeller. The negative dimples in the last three curves are due to the zero axial traction applied at the outflow. The use of this natural boundary condition sets the pressure level at the outflow boundary. The axial traction is given by:

$$t_x = - P + 2\mu_T U_{,x} = 0$$

where t_x is the axial traction and P the pressure. The zero traction defines the pressure level as:

$$P = 2\mu_T U_{,x}$$

Since the axial velocity is still decaying, $U_{,x}$ is negative and the pressure at the exit takes a small negative value.

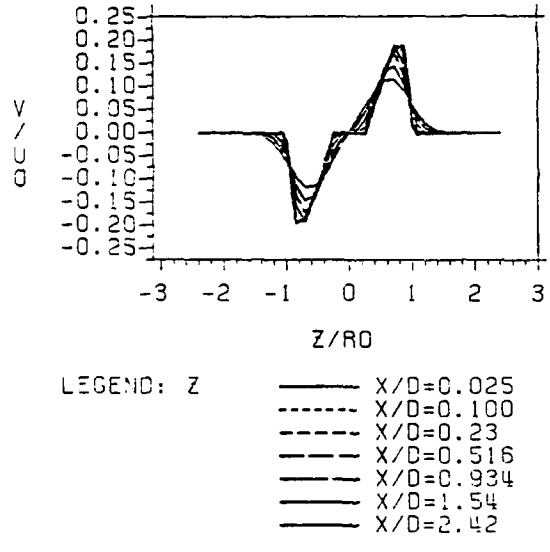

Figure 14: Shear Flow: Swirl Profiles

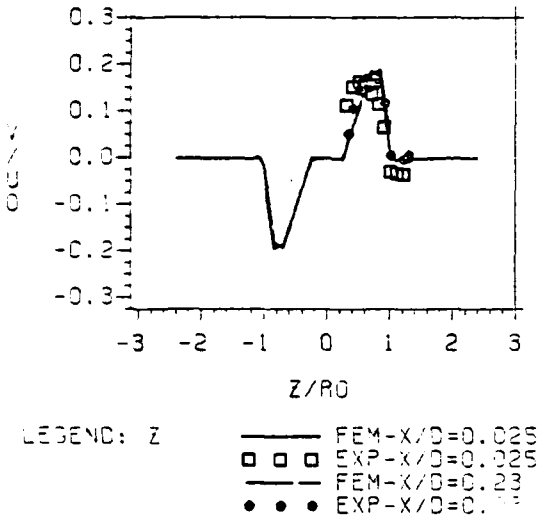

Figure 7: Shear Flow: Swirl

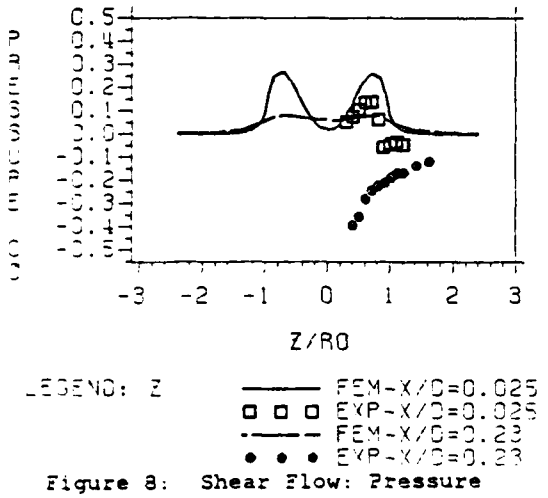

Figure 8: Shear Flow: Pressure

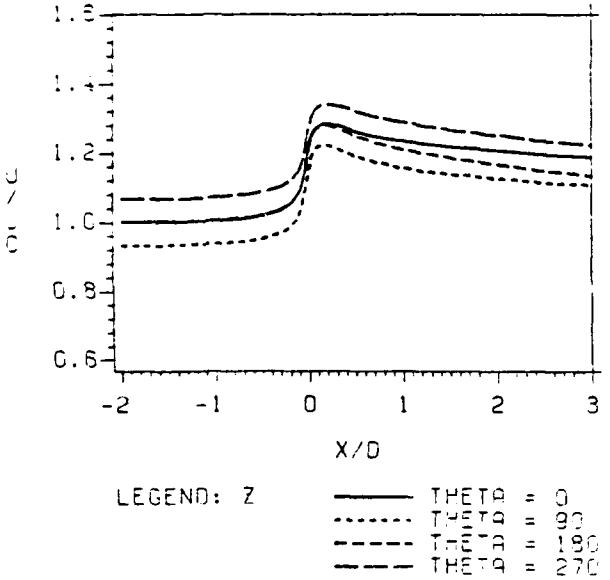

Figure 9: Shear Flow: Axial Velocity Distribution

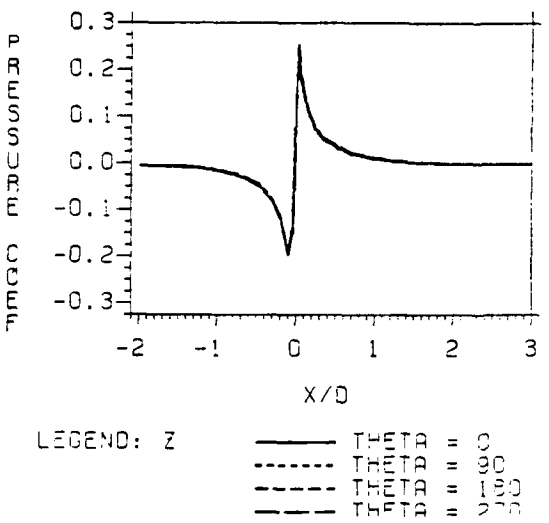

Figure 10: Shear Flow: Pressure Distribution

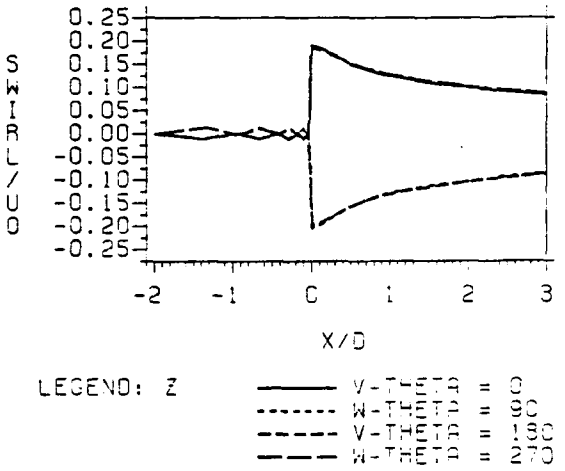

Figure 11: Shear Flow: Swirl Distribution

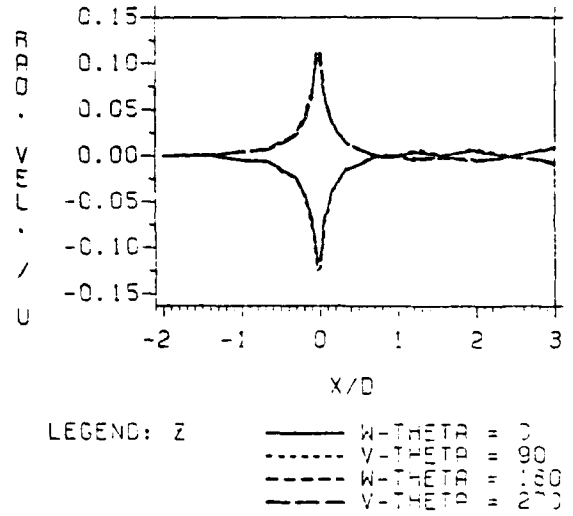

Figure 12: Shear Flow: Radial Velocity Distribution

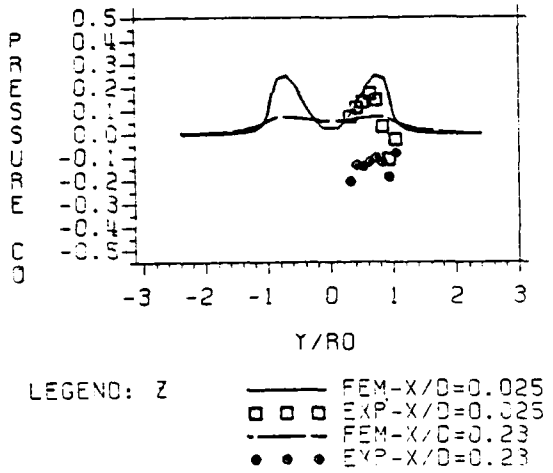

Figure 5: Uniform Flow: Pressure

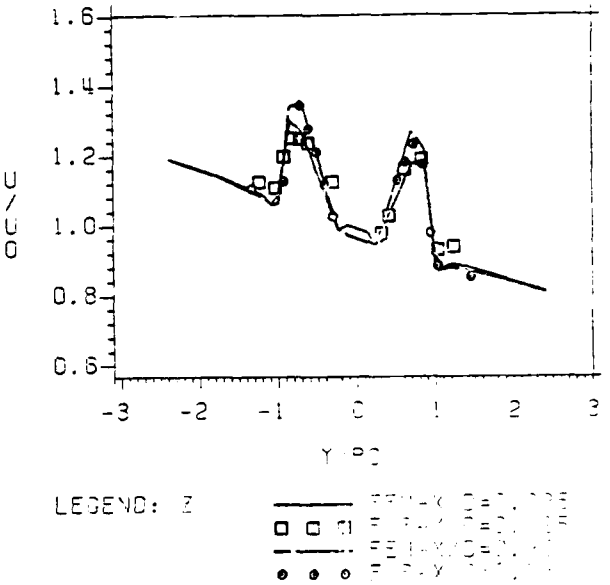

Figure 6: Shear Flow: Axial Velocity

$K_T = T/(\rho_0^* N^2 D^{*4}) = 0.158$

$K_Q = Q/(\rho_0^* N^2 D^{*5}) = 0.0266$

At the inflow and on the freestream shell boundary , U is set equal to the approach shear flow. All other boundary conditions are identical to those used for the uniform flow simulation.

To obtain an initial guess of the velocity field, a 2-D, axisymmetric solution without swirl was produced for a uniform flow and the velocity excess was extracted, rotated on the 3-D grid, and added to the approach shear flow. The system of nonlinear equations was then solved in 2 quasi-Newton iterations requiring a total of 150 minutes of CPU on IBM-3081. No gradual introduction of thrust and torque in the course of the iteration was required as opposed to the work of Refs.[4-6].

Figure (6) compares the experimental and predicted axial velocity profiles along the y axis. The agreement is excellent at x/D = 0.025 and good at x/D = 0.23. On the low speed side of the propeller, less fluid flows through the propeller, and hence, it is subject to more body force per unit mass flow. This results in higher acceleration of the fluid and a larger relative speed increase on the positive side of the y axis compared to the negative side. Figure (7) presents the predicted and experimental swirl profiles along the z axis. Agreement between predictions and experiments is excellent. Figure (8) gives the predicted and experimental pressure profiles along the y axis in the form of a pressure coefficient $C_p = 2(P-P_0)/(\rho U_0^2)$. The experimental profiles have shapes similar to those of the predictions, but the amplitudes do not quite agree at x/D=0.025.

Figures (9) to (12) present predicted axial distributions of the axial component of the velocity, pressure, swirl, and radial velocity. These distributions were taken at a radius equal to 0.85R where the maximum thrust occurs. Figure (9) clearly shows the strong streamwise acceleration of the fluid upstream and downstream for the propeller. The different variations in U at four peripheral location are due to the shear flow. The two curves in the vertical plane display non-symmetrical behavior. This is caused by the swirl that moves high velocity fluid into regions of lower velocity and vice versa. The significant upstream influence of the pro-

A note of caution is required before any comparison with experiments is attempted. While the finite element simulations can accurately represent a free running propeller, the experiments must use a shaft to support and drive the propeller. A body must be placed close to and downstream of the propeller to house the drive train, see Ref.[16]. The housing begins at 0.23 propeller diameters downstream of the disk. The presence of the housing will very likely affect the experimental results from the station located at x/D = 0.23, since this station sits right on the body.

Figure (3) compares the experimental and predicted axial velocity profiles along the y axis. The agreement is excellent at x/D = 0.025 and good at x/D = 0.23.

Figure (4) presents the predicted and experimental swirl profiles along the y axis. It can be seen that the assumed radial distribution of the swirling body force is reasonable, but it has slightly too sharp a peak located too close to the propeller tip. Agreement between predictions and experiments is excellent and constitutes a major improvement over those of Refs.[4-6].

Figure (5) presents the predicted and experimental pressure profiles along the y axis. The pressure is given in the form of a pressure coefficient, $C_p = 2(P-P_0)/(\rho U_0^2)$. These are the first viscous pressure predictions for this type of flow known to the authors. All analysis methods based on the boundary layer equations require the specification of the pressure as input. The agreement with the experiments at x/D=0.025 is good. The pressure predicted at x/D=0.23 is in qualitative agreement with the theory of free running propellers. The experimental profiles at x/D=0.23 have negative values typical of the flow over an obstacle such as the drive housing.

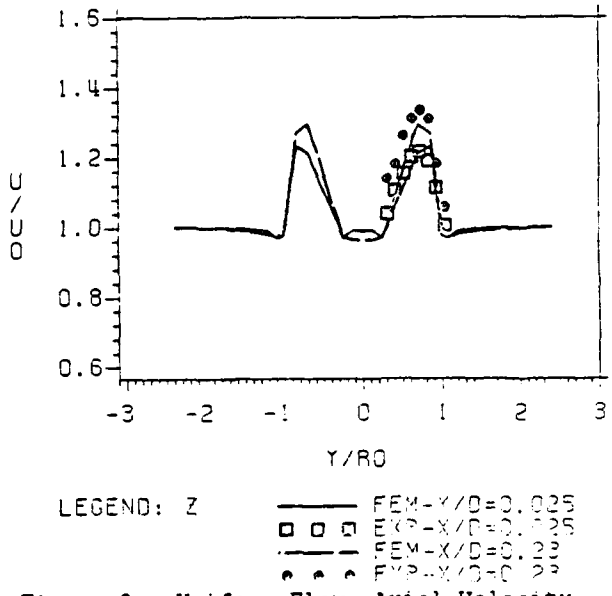

Figure 3: Uniform Flow: Axial Velocity Profile

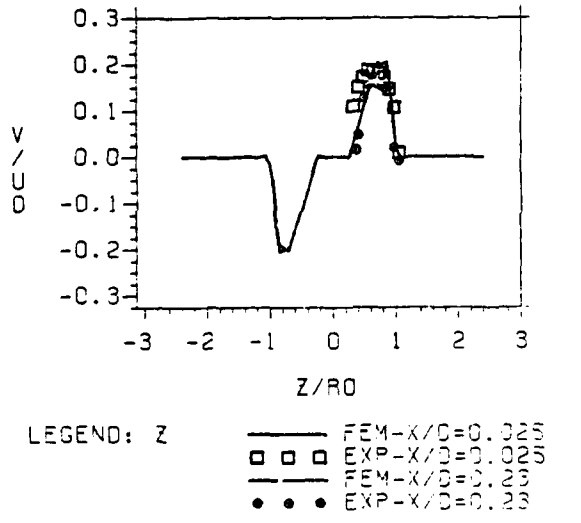

Figure 4: Uniform Flow: Swirl Profile

SHEAR FLOW PAST A PROPELLER

This simulation of a free running propeller in a shear flow corresponds to the experiments of Koto [16]. The characteristics of the flow are as follows:

$U^*_{inf} = 8.52 - 0.67y$ m/s

$U_{inf} = 1 - 0.1588\ y$

$\rho^*_0 = 1.177$ kg/m^3

$D^* = 0.492$ m

N = 1150 rpm

four curves result in clustered distributions well within the margin of uncertainty for this problem. An initial value of $5*10^{-4}$ was judged adequate and used for all subsequent simulations.

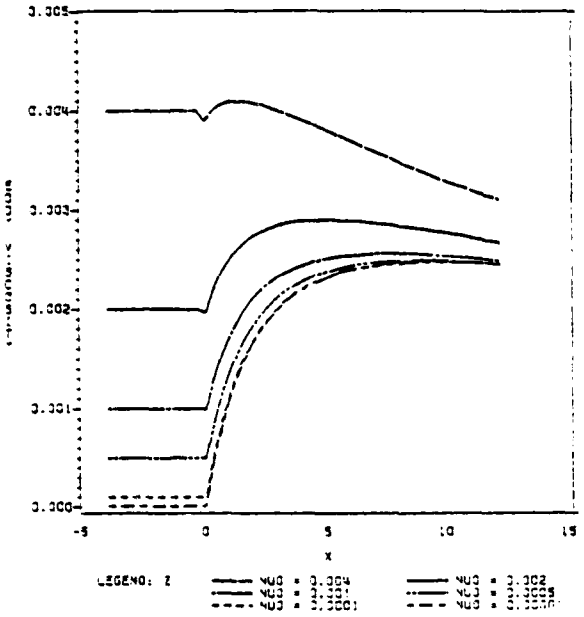

Figure 1: Effect of Initial Value of Eddy Viscosity

COMPUTATIONAL SAVINGS ARISING FROM THE USE OF THE PENALTY METHOD.

To illustrate the computational savings afforded by the use of the penalty method, we present the characteristics of the global stiffness matrix of the 3-D propeller simulations for the penalty and velocity-pressure (mixed) formulations. The mesh has a total of 3768 nodes and 3588 8-noded brick elements.

	Penalty	Mixed
NEQ	10 557	14 145
NEM	10 997 103	19 434 905
MINB	521	687
MAXB	886	1 186

where NEQ is the number of equations, NEM the number of matrix coefficients stored, MINB the average bandwidth of the matrix, and MAXB the maximum bandwidth. The mixed formulation has 34% more unknowns, a bandwidth 32% greater, and stores 77% more matrix coefficients. The Gaussian L-U factorization time is 2 and 5 hours CPU for the penalty and mixed methods repectively (on IBM-3081, using FORTRAN-H extended with optimization level-1). Clearly, the penalty method offers substantial savings.

UNIFORM FLOW PAST A PROPELLER

The characteristics of the flow are as follows:

$U_0^* = 8.52$ m/s

$\rho_0^* = 1.177$ kg/m^3

$D^* = 0.492$ m

$N = 1150$ rpm

$K_T = T/(\rho_0^* N^2 D^{*4}) = 0.150$

$K_Q = Q/(\rho_0^* N^2 D^{*5}) = 0.0279$

The grid is a cylinder with 24 nodes in the axial direction, 14 in the radial direction , and 12 in the peripheral direction. The inflow boundary is located 2 diameters upstream of the propeller, see Fig.(2). The outflow plane stands at 3 diameters downstream of the disk, while the freestream boundary is a cylindrical shell of radius 1.2 diameters. At the inflow, U is set to unit value and V and W are set to zero. On the freestream boundary, U is set to 1 and the y and z tractions to zero. The three components of the traction vector are set to zero at the outflow boundary.

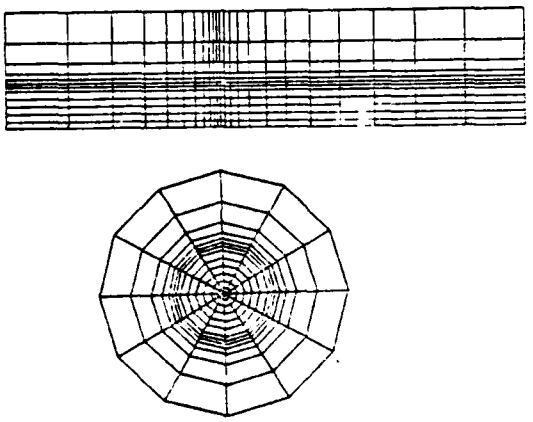

Figure 2: Grid for Propeller Simulation

RESULTS AND DISCUSSION

The turbulence model was programmed and interfaced to the general purpose finite element fluid dynamics program FIDAP [15]. The resulting code can simulate planar, axisymmetric, and three-dimensional turbulent free shear flows.

NONDIMENSIONALIZATION

All calculations were performed with a nondimensional form of the equations of motion for the conditions of Ref.[16]. Reference values are selected for the velocity (U_0^*), length (L_0^*), and pressure (P_0^*) to obtain the following dimensionless variables (the star denotes a dimensional variable):

$$x_i = x_i^*/L_0^*$$
$$U_i = U_i^*/U_0^*$$
$$P = (P^*-P_0^*)/(\rho U_0^2)$$
$$\mu_T = \mu_T^*/(\rho U_0^* L_0^*) = 1/Re_{\mu_T}$$
$$f = f^*/(U_0^2/L_0^*)$$
$$\rho = \rho/\rho_0^* = 1$$

INITIAL VALUE FOR THE EDDY VISCOSITY

The absence of solid walls or aftbody upstream of the propeller in the present, idealized flow problem results in an undisturbed "inviscid", uniform or shear approach flow making difficult the determination of the initial condition for the turbulence model. The flow through and past a propeller has many of the characteristics of a turbulent jet [17]. Hence, an indication of the magnitude of μ_T may be obtained from the standard jet formula for the eddy viscosity [17]:

$$\nu_T = 0.025\ r_{1/2}\ \Delta U$$

where $r_{1/2}$ is the halfwidth of the layer and can be taken as $r_{1/2}$=R, the radius of the propeller and ΔU is the characteristic velocity excess determined from a simplified inviscid, one-dimensional analysis of the propeller [18]:

$$\Delta U^* = [\ 2T^*/(\rho^* A) + V_0^{*2}\ ]^{1/2} - U_0^*$$

The following data applies to the uniform flow case of Ref.[16]:

$$R^* = 0.246\ m$$
$$U_0^* = 8.52\ m/s$$
$$T^* = 2.914\ N$$
$$A^* = 0.19\ m^2$$
$$\rho^* = 1.177\ kg/m^3$$

$$\Delta U^* = 1.41\ m/s$$

A rough estimate of the eddy viscosity downstream of the propeller is in dimensionless form:

$$\mu_T = \nu_T^*/(DU_0) = 0.002$$

There remains to select an initial value for the eddy viscosity. Assuming that the Prandtl-Kolmogorov relationship holds we have:

$$\nu_{T_{init}}^* = 0.2\ k_0^{1/2}\ R$$

where c=0.2 (the value for jets) and k_0 is the turbulence intensity upstream of the propeller. The corresponding dimensionless form is

$$\nu_{T_{init}} = \nu_{T_{init}}^*/(U_0 D) = 0.1\ k_0^{1/2}/U_0$$

From the experiments of Ref.[16] we have

$$k_0^{*1/2}/u_0^* = 0.01$$

and an estimate of the initial eddy viscosity is finally

$$\nu_{T_{init}} = 0.001$$

To assess the validity of this analysis and to investigate the effect of the choice of the initial value on the eddy viscosity distribution, simulations were performed for the uniform flow of Ref.[16]. The calculations were done for an axisymmetric flow without swirl.

Figure (1) shows that low values of μ_T, in the range 10^{-5} to 10^{-3}, produce similar results with a peak eddy viscosity of 0.0025, a value in good agreement with our rough estimate of 0.002. Higher initial values produce distributions that are probably too high. The bottom

where R_i are the residuals, a measure of the quality of the approximate solution used. The Galerkin method reduces this error to zero, in a weighted sense, by making the residuals orthogonal to some set of functions. The weighting functions, δU_i, must satisfy the continuity equation. The continuity equation constraint is enforced by use of a penalty method. The resulting weak formulation is given by [7,11]:

$$\int_D \{\delta U_i \rho U_j U_{i,j} + \delta U_{i,j} \mu_T (U_{i,j} + U_{j,i}) + \delta U_i \rho f_i\} d\Omega$$

$$\int_D U_{i,i} \delta U_{i,i} \, dD = \int_S \delta U_i t_i \, dS \quad (10)$$

Here λ is a positive number whose value affects the accuracy of the solution, while δU_i may be interpreted as a virtual velocity, and eq.(10) is similar to the principle of virtual work of solid

The divergence theorem was applied to the pressure and viscous terms to reduce the differentiability requirement on the velocity by transfering some of the derivative from U_i to δU_i, and to introduce the natural boundary conditions involving the surface tractions or forces t_i:

$$t_i = \{-P + \mu_T (U_{i,j} + U_{j,i})\} n_j$$

The pressure does not appear explicitly in eq.(10); it appears only implicitly through the surface integrals on the right hand side of eq.(10). The only unknowns are the velocity components. This results in significant computational savings. Once the velocity field is obtained by solving eq.(10), the pressure may be computed in a post processing step from the following relationship [7,11]:

$$P = -\lambda U_{i,i} \quad (11)$$

Convergence of the solution of the penalty formulation to the true solution, as $\lambda \to \infty$, can be proved [12]. A value of λ of 10^6 to 10^8 usually proves effective.

For reasons of computational economy, we use the trilinear velocity, constant pressure element [11]. This element, under certain circumstances may suffer from spurious pressure solutions. Our experience with this element indicates that it is a fairly reliable element for the problems treated here. No spurious pressure solutions were observed.

GENERAL SOLUTION PROCEDURE

The formulation results in a system of nonlinear algebraic equations of the form:

$$[K(U, \mu_T(U))] \, U = F$$

where K is the global system matrix, U is the global vector of unknowns, and F is the global vector of body forces and boundary conditions.

This system of equations may be solved by a combination of methods: successive substitution, Newton-Raphson, and quasi-Newton methods [13]. The quasi-Newton procedure converges as fast as the full Newton method, but the cost of one quasi-Newton iteration is about 10 to 15% of that of a Newton iteration. The following iteration strategy was found suitable throughout this study: starting from a first guess for the velocity field, the quasi-Newton method is used to iterate until convergence. The eddy viscosity distribution is updated at each iteration by solving eq.(6) using the current velocity distribution to evaluate the coefficients of the ordinary differential equation. The linearized system of equations is very large and is solved by direct Gaussian decomposition in a compacted, skyline, out of core solver [14].

$$dv_T/dx = 0.5(Y_2 - v_T dY_1/dx - v_T^2 Y_3)/Y_1 \quad (6)$$

where

$$Y_1 = \int\!\!\int_A U\gamma^2/(C_2^2 L)\, dA$$

$$Y_2 = \int\!\!\int_A \gamma[(U_{,y})^2+(U_{,z})^2+(V_{,z}+W_{,y})^2]\, dA$$

$$Y_3 = \int\!\!\int_A \gamma a_2/(c_2^3 L)\, dA$$

It now remains to specify the length scale L. Following Ref.[9] we adopt:

$$L = [(Y_{1/2}^a\, Z_{1/2}^a)/(Y_{1/2}^a + Z_{1/2}^a)]^{1/a}$$

with a = 1.89. This ensure correct dependence for the limiting cases of planar and axisymmetric flows. Equatio (6) is an initial value problem for the kinematic eddy viscosity v_T. The only data required is an initial condition for v_T at the upstream inflow boundary, a value that can be easily estimated for most flows. One significant advantage of the present model is the absence of the diffusion of TKE, a most difficult term to model.

The present model was calibrated on the simple, well documented turbulent flow problem of the far field of a round jet issuing into still surroundings. This flow has an analytical solution [&R11.] *for the velocity field*, and the value of the eddy viscosity is known and constant. The integrals are evaluated exactly and with the assumption of turbulence equilibrium the constants are determined to be [7]:

$$a_2 = 0.519 \qquad c_2 = 0.154$$

MODELING OF THE PROPELLER

The propeller is modeled by a disk of radius equal to the propeller radius and of thickness Δx, roughly equal to the physical thickness of the propeller. The thrust and torque are allowed to vary radially but are constant in the tangential direction. Little is known about the detailed radial thrust and torque distributions of a given propeller. Generally, one only knows the global values of total thrust and torque. For simplicity we use a trapezoidal distribution given by:

$$\begin{aligned}
t(r) &= 0 && r \text{ in } [0,r1] \\
t(r) &= t_m(r-r_1)/(r_2-r_1) && r \text{ in } [r_1,r_2] \\
t(r) &= t_m && r \text{ in } [r_2,r_3] \quad (7) \\
t(r) &= t_m(R-r)/(R-r_3) && r \text{ in } [r_3,R] \\
t(r) &= 0 && r>R
\end{aligned}$$

where t_m is the maximum value of the thrust and R is the radius of the propeller. Values of r_1, r_2, and r_3 were set to 0.25R, 0.7R, and 0.85R respectively. These values result in distributions similar to those of Refs.[4-6]. The same form is adopted for the dictribution of the force s producing the swirl. Its maximum value is denoted by s_m. The upstream face of the propeller disk is located at $x = -\Delta x$, while the backface of the propeller is located at x = 0.0. These distributions are integrated to yield the global thrust and torque of the propeller :

$$T = 0.3075 * 2\,\Pi * R^2 * t_m \quad (8)$$

$$Q = 0.2218 * 2\,\Pi * R^3 * s_m \quad (9)$$

Given values of the global thrust and torque, the values of t_m and s_m are determined form eqs.(8) and (9).

SOLUTION ALGORITHM

PENALTY FORMULATION

Details of the weak Galerkin formulation are readily available for penalty function formulations [11]. Thus, only an outline of the technique is presented here.

Substitution of an approximate solution (U^*,P^*) into eqs.(1) and (2) yields a set of residual equations of the form:

$$\text{Momentum} : f_1(U^*,P^*) = R_1$$

$$\text{Continuity} : f_2(U^*) = R_2$$

MODELING OF THE PROBLEM

EQUATIONS OF MOTION

The mean flow equations in cartesian coordinates are given by:

$$U_{i,i} = 0 \tag{1}$$

$$\rho U_j U_{i,j} = - P_{,i} + \rho f_i + [\mu_T (U_{i,j} + U_{j,i})]_{,j} \tag{2}$$

where μ_T is the turbulent eddy viscosity, and f_i are body forces representing the effects of the propeller disk.

TURBULENCE MODEL

Following Refs.[4-6] a simple turbulence model is used, since little experimental data is available for this type of problem on which to base more elaborate models. An integrated form of the TKE equation is used (details of the algebraic manipulations are contained in Ref.[7]):

$$d(\iint_A \rho U k \, dA)/dx = \iint_A \nu_T [(U_{,y})^2 + (U_{,z})^2 + (V_{,z} + W_{,y})^2] \, dA + \iint_A \varepsilon \, dA \tag{3}$$

In order to close the model, the TKE must be related to the eddy viscosity $\mu_T = \rho \nu_T$. This is done through the use of the Prandtl-Kolmogorov relationship [8]

$$\nu_T = c_2 \, k^{1/2} \, L \tag{4}$$

Assuming that laminar dissipation is important only in the inertial sub-range, dimensional consistency dictates that the viscous dissipation be modeled as [8]:

$$\varepsilon = a_2 \, k^{3/2} / L \tag{5}$$

where L is a characteristic length scale of the shear layer, and a_2 and c_2 are constants. Physically, all integrands in eq.(3) are sufficiently well behaved to ensure boundedness of the integrals. The assumption that the eddy viscosity is constant over the cross section of the flow is a well documented behavior for free shear flows. In fact, the eddy viscosity is constant over most of the shear layer and decays to zero only as the radial distance, r, from the x-axis goes to infinity. In order to preserve this behavior and ensure boundedness of the integrals in the modelled integrated equation, we introduce a distribution function, γ, representing the distribution of μ_T across the layer. It is closely related to the actual intermittency of the turbulent flow. The following form, obtained from a nonlinear least squares fit to intermittency data for a turbulent boundary layer over a flat plate and turbulent plane and round jets was found satisfactory:

$$\gamma = \gamma_y \gamma_z$$

where

$$\gamma_y = 0.5 \, (1 - \mathrm{erf}(1.98 Y / Y_{1/2} - 3.42))$$
$$\gamma_z = 0.5 \, (1 - \mathrm{erf}(1.98 Z / Z_{1/2} - 3.42))$$

and $Y_{1/2}$ and $Z_{1/2}$ are the half-widths of the shear layer along the y and z axes respectively. The half-widths are defined by the points on the axis where :

$$(U - U_{inf})/(U - U_{inf})_{max} = 0.5$$

In this expression, U_{inf} is the free stream approach flow velocity which can be non-uniform.

It should be noted that the particular form of the distribution function used is not critical. Choosing different algebraic forms will simply result in slightly different values of the constant a_2 and c_2.

Upon substitution of eq.(4) and eq.(5) into eq.(3), the modeled integrated TKE equation takes the form:

INTRODUCTION

Detailed analysis of the 3-D, turbulent flow produced by a propeller/body combination is of interest in a number of practical applications. Examples include the influence of the propeller on the body pressure distribution, the prediction of the near-wake profiles, cyclic loading to produce vibrations and the influence of a downstream surface on a propeller and vice versa, to name a few. Until recently, only approximate treatments were available involving one or more of the following restrictive assumptions: the flow was assumed inviscid; the propeller was represented as an actuator disk with constant thrust; the flow was taken as laminar and/or the effects of the propeller on the flowfield were assumed small enough to permit linearization of the equations of motion. Refs.[1-3] are representative.

The numerical solution procedure reported in Refs.[4-6] had as its goal the development of a realistic treatment, holding simplifying assumptions and approximations to a minimum. The work was based on the full, axisymmetric, mean (in the turbulence sense), unsteady Navier-Stokes equations. In order to place some bounds on the scope of the effort at that time, however, some simplifications were necessary. The first was the assumption of an actuator disk model for the propeller, although arbitrary radial variations of thrust were allowed. Second, the flow was taken as axisymmetric. Third, turbulent transport processes were described by an integrated, turbulence-kinetic-energy (TKE) model, which was used to predict an eddy viscosity distribution. The unsteady equations of motions were cast in terms of a stream function, one vorticity component, and the peripheral velocity. Comparison of the predictions of this procedure with laboratory data for an axisymmetric flow, showed good agreement for the axial velocity component. The swirl velocity component predictions were consistently too low.

From the point of view of direct applications to problems of practical interest, the biggest limitation to the analysis described above is its restriction to two-dimensional, axisymmetric flows. Actual propeller-driven vehicles have either a three-dimensional body near the propeller and/or appendages that render the flow three-dimensional. For many cases, the assumption of an actuator disk representation of the propeller remains appropriate while the restriction to axisymmetric flow does not. Furthermore, the jump to trying to treat the three-dimensional, cyclicaly unsteady problem with individual blades and their thin boundary layers and wakes is too great to be attempted in one step at this time.

The present work is part of a step-by-step approach to the development of a computational method for analysis of propeller flowfields with three-dimensional inflows and the effects of appendages in situations of increasing complexity and practical realism. The fully elliptic, three-dimensional, time averaged, steady state, primitive variables Navier-Stokes equations are solved by a Penalty Finite Element Method because of its ease of handling complicated geometries and its simplicty for implementing a variety of boundary conditions. Turbulence modeling is done through a generalization of the integrated TKE model of Refs.[4-6].

A NAVIER-STOKES CALCULATION OF 3-D, TURBULENT FLOW NEAR A PROPELLER IN A SHEAR FLOW

by

D. H. Pelletier * and J. A. Schetz **

Aerospace and Ocean Engineering
Virginia Polytechnic Institute and State University
Blacksburg, VA 24061

Abstract

A numerical procedure based on the primitive variable Navier-Stokes equations is applied to the simulation of the three-dimensional flow near a propeller in a shear flow. The Navier-Stokes equations are solved by a Penalty Finite Element Method. The propeller is modelled as an actuator disk, and the direct simulation of a given propeller is considered in detail. Turbulent transport is modeled by an integrated Turbulent Kinetic Energy equation. This approach results in a robust numerical algorithm. Detailed comparison with wind tunnel measurements show good prediction of velocity and pressure. The high accuracy of the swirl prediction is a major improvement over previous analyses.

NOMENCLATURE

- A ... cross section of the flowfield and area of the propeller
- a_2 .. constant in the turbulence model
- c_2 .. constant in the turbulence model
- D ... domain of solution and propeller diameter
- κ ... turbulence kinetic energy
- K_Q .. torque coefficient
- K_T .. thrust coefficient
- N ... rotational speed of the propeller
- n_j .. unit outward normal
- P ... pressure
- Q ... torque of the propeller
- $r_{1/2}$ half-width of shear layer
- Re .. Reynolds number
- s ... radial distribution of swirl force
- S ... boundary of the domain D
- t ... distribution of thrust
- t_i .. surface traction vector
- T ... thrust of the propeller
- U_i .. velocity vector
- U_{inf} upstream approach flow
- ρ ... density of the fluid
- ε ... turbulence viscous dissipation
- λ ... penalty parameter

* Adjunct Professor, member AIAA, also Applied Mathematics, Ecole Polytechnique de Montreal, Montreal, Canada

** Professor and Dept. Head, Associate Fellow AIAA.

AIAA'85

AIAA-85-0365

A Navier-Stokes Calculation of 3-D, Turbulent Flow Near a Propeller in a Shear Flow

D. H. Pelletier and J. A. Schetz,
Virginia Polytechnic Institute and
State Univ., Blacksburg, VA

AIAA 23rd Aerospace Sciences Meeting

January 14-17, 1985/Reno, Nevada

Appendix

Reprint of Publication

6. Schetz J. A. and Figard R. L., "Numerical Solution of the Flow Near the Rotor of a Wind Turbine," Journal of Energy, Vol. 6, No. 2, 1982.

7. Pelletier D. H., "Finite Element Solution of the Navier-Stokes Equations for 3-D Turbulent Free Shear flows," Ph.D. Dissertation, Aerospace and Ocean Engineering Dept., Virginia Polytechnic Institute and State University, Blacksburg,VA.

8. Rodi W., Turbulence Models and Their Application in Hydraulics, International Association for Hydraulic Research, Delft, The Netherlands, 1980.

9. Sforza P. M., Steiger M. H. and Trentacoste N., "Studies on Three-Dimensional Viscous Jets," AIAA J., Vol. 1, No. 5, 1966.

10. Hinze J. O., Turbulence, Second Edition, Mc Graw-Hill, 1975.

11. Reddy J. N., "Penalty-Finite-Element Analysis .. 3-D Navier-Stokes Equations," Comp. Meth. Appl. Mech. Eng., Vol. 35, 1982.

12. Reddy J. N., "On Penalty Function Methods in the Finite Element Analysis of Flow Problems," Int. J. Num. Meth. Fluids, Vol. 2, 1982.

13. Engelman M. S., Strang G. and Bathe K.-J., "Application of Quasi-Newton Methods in Fluid Mechanics," Int. J. Num. Meth. Eng., Vol. 17, 1981.

14. Hasbani Y. and Engelman M. S., "Out of Core Solution of Linear Equations with a Non-symmetric Coefficient Matrix," Comp. and Fluids, Vol. 7, 1979.

15. Engelman M. S., "FIDAP: A Fluid Dynamics Analysis Program," Adv. Eng. Soft., Vol. 4, 1982.

16. Kotb M. A., "Experimental Investigation of 3-D Turbulent Free Shear Flows Past Propellers and Windmills," Ph.D. Dissertation, Aerospace and Ocean Engineering Department, Virginia Polytechnic Institute and State University, October 1984.

17. Schetz J. A., Foundations of Boundary Layer Theory for Momentum, Heat, and Mass Transfer, Prentice-Hall, 1984.

18. Li W.-H. and Lam S.-H., Principles of Fluid Mechanics, Addison Wesley, 1964.

ACKNOWLEDGEMENT

This work is supported by the Office of Naval Research with Dr. Choung Lee as Technical Monitor.

Distribution List

Defense Tech. Info. Center Cameron Station Alexandria, VA 22314	12 copies
Office of Naval Research 800 No. Quincy St. Arlington, VA 22217	3 copies

END

FILMED

9-85

DTIC